

1. Report No. NASA TN D-6931	2. Government Accession No.	3. Recipient's Catalog No.	
4. Title and Subtitle EFFECTS OF EXPERIMENTALLY MEASURED PRES- SURE OSCILLATIONS ON THE VIBRATION OF A SOLID ROCKET MOTOR		5. Report Date November 1972	
		6. Performing Organization Code	
7. Author(s) James A. Schoenster and Harold B. Pierce		8. Performing Organization Report No. L-8417	
		10. Work Unit No. 114-08-13-03	
9. Performing Organization Name and Address NASA Langley Research Center Hampton, Va. 23365		11. Contract or Grant No.	
		13. Type of Report and Period Covered Technical Note	
12. Sponsoring Agency Name and Address National Aeronautics and Space Administration Washington, D.C. 20546		14. Sponsoring Agency Code	
		15. Supplementary Notes	
16. Abstract <p>Results are presented of firing a Nike rocket against a backstop for the purpose of obtaining pressure fluctuations in the rocket case and determining their relationship to structural vibrations of the case. Special care was required to obtain these pressure fluctuations because of the much higher static pressure generated in the rocket. The results showed that very small pressure fluctuations within the rocket case can cause significant vibration levels. A previously observed high frequency (i.e., above 10 kHz) was shown to decrease with time before completely disappearing at about 1 second of burning time. The vibration of the case itself is probably related to the longitudinal structural modes at frequencies below 500 Hz and is dependent on local structural conditions at frequencies above this value.</p>			
17. Key Words (Suggested by Author(s)) Solid-rocket-motor vibrations Random vibration analysis		18. Distribution Statement Unclassified - Unlimited	
19. Security Classif. (of this report) Unclassified	20. Security Classif. (of this page) Unclassified	21. No. of Pages 45	22. Price* \$3.00

* For sale by the National Technical Information Service, Springfield, Virginia 22151

I

EFFECTS OF EXPERIMENTALLY MEASURED PRESSURE OSCILLATIONS ON THE VIBRATION OF A SOLID ROCKET MOTOR

By James A. Schoenster and Harold B. Pierce
Langley Research Center

SUMMARY

This report presents results of firing a Nike rocket against a backstop for the purpose of obtaining pressure fluctuations in the rocket case and determining their relationship to structural vibrations of the case. Special care was required to obtain the pressure fluctuations which are superimposed on the much higher (several orders of magnitude) static pressure which generates the thrust of the rocket. Vibrations of the case were obtained at the nozzle end and the forward thrust face of the rocket motor. Oscillatory data obtained from this firing are random in nature and advantage was taken of this condition to use not only the basic random-vibration analysis techniques but also the higher order correlation function coefficient to study the structural behavior.

Results from analysis of the data show that for the Nike rocket, very small pressure fluctuations can cause significant vibrations in the structure. A previously reported phenomenon of high responses at frequencies above 10 kHz was also observed and was determined to be an oscillation decreasing in frequency with time before completely disappearing at about 1 second of burning time. The vibration of the rocket case is probably related primarily to longitudinal structural modes at frequencies below 500 Hz, whereas at frequencies above 500 Hz the measured vibration was dependent on local structural conditions.

INTRODUCTION

The combustion of the propellant in a solid rocket motor is a major source of dynamic loads to both the rocket motor and the payload. Surveys of work in the structural dynamics of solid-propellant rockets (refs. 1 and 2) indicate that although much work has been conducted into the interaction of combustion and mechanical vibrations, the problem is far from being resolved. Significant progress has been made in analytical techniques combining combustion effects with dynamics of vehicle (refs. 3 and 4); however, the results from this work were analytically evaluated for combustion times less than one-fourth of the entire burn time of a rocket motor and have not been verified experimentally. Some work (ref. 1) has also been directed toward understanding and

suppressing various forms of potentially destructive acoustic instabilities when they are found during the development of new solid rocket motors. Once structural integrity of a new motor is assured, little effort is expended in establishing environmental specifications based on residual pressure fluctuations unless some problem develops with a vehicle using this motor. Measurements of the vibratory response during the combustion period have been made on vehicles using such rocket motors as the Nike M88, X-248, Sidewinder-Arcas, and the third stage of Minuteman (refs. 5 to 8). Some of the measured vibrations have been associated with acoustic chamber pressure oscillations through a similarity in frequencies (refs. 6 and 8) but no direct relationship between magnitude of pressure fluctuations and magnitude of vibration response has been established, primarily because of the lack of detailed measured pressure fluctuations. Although there is a significant amount of difficulty in obtaining such measurements, as indicated in references 5 and 9, the chamber pressure fluctuations and the understanding of their relationship to structural vibrations is very significant in developing reasonable and adequate environmental specifications (for example, ref. 10).

As part of a continuing program at Langley Research Center to develop techniques for predicting vibration environments – which includes measurements on a rocket fired in a unique test stand (ref. 5) and on the same vehicle in flight – a solid-propellant Nike rocket was fired against a backstop. The purpose of this report is to present results from this test showing the relationship of the chamber pressure fluctuations during combustion and the structural vibrations resulting from these fluctuations, particularly the transmission of dynamic loads through the case structure. Statistical estimate parameters are used to analyze and discuss the results.

SYMBOLS

Values are given in both SI and U.S. Customary Units. The measurements and calculations were made in U.S. Customary Units.

B	bandwidth, Hz
f	frequency, Hz
g	acceleration of gravity, 9.807 m/sec ²
k	number of statistical degrees of freedom
m	maximum number of time-lag values

n	sample size (number of items in a sample time history)
$p(x)$	probability-density function
R	gas constant
$R_x(\tau), R_y(\tau)$	autocorrelation function of x and y , respectively
$R_{xy}(\tau)$	cross-correlation function
T	record length, seconds
T_1	absolute temperature, K
t	time, seconds
$x, x(t), y, y(t)$	amplitude, g units or N/m^2
γ	specific heat ratio
ϵ	sample interval, seconds
λ	wavelength, cm
$\rho_{xy}(\tau)$	correlation function coefficient
σ_x	root-mean-square value, g units or N/m^2
τ	time lag, seconds

APPARATUS AND TEST CONDITIONS

Description of Rocket Motor in Test Stand

A Nike type M88 solid-propellant rocket motor was the test vehicle. The rigid backstop and horizontal test stand in which it was fired are shown in figure 1. The rocket motor was attached to the backstop through a thrust cone and load cell. The rocket motor, thrust cone, and load cell are shown in figure 2 before the rocket motor was moved forward and bolted to the thrust cone. The rocket motor was supported at three positions along its length by vee-blocks. The vee-blocks (figs. 1 and 3) prevented lateral or verti-

cal motion of the motor but permitted longitudinal expansion of the motor during firing by means of rollers in contact with the motor case (fig. 3).

Description of Instrumentation

The instruments used in the horizontal ground firing were of three types: pressure transducer, vibrometer, and load cell. Listed in table I are the linear frequency range, the linear amplitude range, and the calibrate factors for each of the instruments. All data obtained from these instruments were recorded on an FM magnetic tape recorder and each instrument is numbered according to its tape channel number.

Pressure transducers.- Four pressure transducers were used in the test. One was a strain-gage type used to measure the time history of the overall chamber pressure, and the remaining three were acceleration-compensated crystal pressure transducers ranged to measure only the fluctuations in chamber pressure. Strain-gage pressure transducer 4 was installed in a fixture as shown in figure 4, and the assembly was mounted on the dome of the rocket motor as shown in figure 2. In addition to the heat protection provided by the length of path from the transducer to the interior of the motor, further protection was provided by an 0.8-mm- (0.03-inch-) thick layer of room-temperature-vulcanized rubber (RTV) bonded to the diaphragm of the pressure transducer.

Two of the crystal pressure transducers, numbered 11 and 13, were located on the forward dome of the rocket motor at the same radial distance from the center line of the motor but 180° apart (fig. 2). The third, crystal pressure transducer 9, was located on the convergent portion of the motor nozzle (fig. 3) exactly in line with dome transducer 13. Pressure transducers 11 and 13 were each mounted in a fixture of the type shown in figure 5. This assembly is shown approximately twice normal size as it is mounted in the rocket motor dome. A boss was added to the exterior surface of the dome and machined so that when the transducer mounting fixture was torqued in place, the sensing portion of the transducer assembly was flush with the interior surface of the rocket motor dome. The transducer mounting fixture protected the transducers from the temperature environment at the rocket motor dome and also provided the electrical isolation desirable when the transducers were used with charge amplifiers. At the nozzle, the high-velocity flow made the rocket motor environment more severe than at the dome, and it was necessary that pressure transducer 9 be protected by the fixture shown in figure 6. The additional protection required for transducer 9 lowered its linear frequency response to 2500 Hz as compared with 5000 Hz for transducers 11 and 13 (table I). A procedure similar to that used for transducers 11 and 13 was used to mount transducer 9 in the nozzle.

Vibrometers.- Vibrometers 1 and 3 were mounted at the nozzle end of the rocket motor (fig. 3). Vibrometer 1 was mounted on the fixture holding pressure transducer 9, and vibrometer 3 was mounted in a longitudinal direction against a block bolted to the aft

end of the rocket motor. Vibrometers 5 and 7 were mounted at the dome end of the rocket motor, with vibrometer 7 being mounted on pressure transducer 13 (fig. 2). Vibrometer 5 is not clearly shown in figure 2, but it is mounted in a longitudinal direction in a cutout in the thrust cone which, during the firing, is bolted to the thrust face of the rocket motor.

All vibrometers were crystal accelerometers mounted on thermal-electrical isolation studs and were used with charge amplifiers. This vibration measurement system was checked on a calibration shaker to 10 kHz and the amplitude response was down 1.2 dB at that frequency.

Load cell.- Load cell 6 was of the strain-gage type. It is shown in figure 2 mounted to the forward end of the thrust cone and is oriented to measure the thrust of the rocket motor against the backstop.

Data-Analysis Techniques

Experimental data were analyzed by using five methods of interpretation: (1) time history; (2) power spectral analysis; (3) autocorrelation function, which at zero time delay is the mean-square value; (4) amplitude histogram; and (5) cross-correlation function and correlation function coefficient. The procedures used in the first four methods are described in references 5 and 10, with the major estimate parameters listed in table II. The fifth method, cross-correlation function and correlation function coefficient, is used to study the linear dependence between two signals. The cross-correlation function may be described by the equation

$$R_{xy}(\tau) = \lim_{T \rightarrow \infty} \int_0^T x(t)y(t+\tau) dt \quad (1)$$

where

$R_{xy}(\tau)$ cross-correlation function

T record length

x(t) time-dependent variable

y(t) time-dependent variable

τ time lag

t time

By using the cross-correlation function and the autocorrelation function for both variables $x(t)$ and $y(t)$, the correlation function coefficient is described by the equation

$$\rho_{xy}(\tau) = \frac{R_{xy}(\tau)}{\sqrt{R_x(0) R_y(0)}} \quad (2)$$

where

$\rho_{xy}(\tau)$ correlation function coefficient

$R_{xy}(\tau)$ cross-correlation function

$R_x(0)$ autocorrelation function of x evaluated at $\tau = 0$

$R_y(0)$ autocorrelation function of y evaluated at $\tau = 0$

The value of the correlation function coefficient is bounded by limits of $-1 \leq \rho_{xy}(\tau) \leq 1$ for stationary random vibration of linear systems. The value of the correlation coefficient is either +1 or -1 for completely correlated signals and zero for completely uncorrelated signals. If the correlation coefficient has a value other than ± 1 and there is reason to believe the signals are correlated, then one or more of three possible conditions exist: (1) uncorrelated signal noise occurring in either the input or the output measuring systems or in both; (2) nonlinear system relationship between the two signals; (3) additional inputs to either of the signals which are uncorrelated to the initial input. The effect of any one of these three conditions is to reduce the magnitude of the correlation function coefficient. Although additional computations can be performed to evaluate the effect of each of the preceding conditions, this study only investigates relationships indicated by the correlation function coefficient. The additional computations are quite extensive and require a quality of data not available from this test. Further information on both the cross-correlation function and correlation function coefficient may be found in such sources as references 11 and 12.

The maximum value of the correlation function coefficient was calculated for several combinations of signals in octave bandwidths of frequency. Octave bandwidths of frequency were selected for two reasons: (1) It was an objective of this test to investigate the transmission of loads through a structure as a function of frequency and (2) it is necessary to use octave bandwidths or less to obtain useful values of the cross-correlation coefficient in structural vibration. An objective of the test, mentioned in reason (1), was to determine the effect on the structure of the pressure oscillations at the aft end of the vehicle relative to the pressure oscillations at the forward end of the vehicle. The second reason for selecting octave bandwidths follows from a study of cross correlation in structural

vibration (ref. 12), where it was determined, both theoretically and experimentally, that information can be obtained from one-octave-band analysis which is not available in broadband correlations. It was demonstrated that the velocity of propagation of flexural waves in a structure (dispersive waves) varies with frequency which causes shifts in the correlation peaks.

A normal-distribution curve is superimposed on the plots of amplitude histograms. The probability-density function for a normal distribution with a zero mean value is

$$p(x) = \frac{1}{\sigma_x \sqrt{2\pi}} e^{-\frac{1}{2} \left(\frac{x}{\sigma_x} \right)^2}$$

where

$p(x)$ probability-density function

σ_x root-mean-square value

x amplitude

The maximum value of the histogram is normalized to the maximum value of the normal-distribution probability-density function, and the root-mean-square value of the variable is used to match the experimental data to the calculated curve. The normal-distribution probability-density function is plotted from minus four times the root-mean-square value to plus four times the root-mean-square value.

RESULTS AND DISCUSSION

The results from firing the rocket motor are presented in figures 7 to 14. Listed in table II are the data-analysis estimate parameters for two time periods during the burning of the rocket motor. Measurements from the load cell, pressure transducers, and vibrometers are presented on oscillograph records for the entire burn time in figure 7. Records with higher resolution than those shown in figure 7 were used to obtain some of the results presented in this report. The vertical lines connected by arrows in figure 7 show the time periods which were analyzed, and at the bottom of the figure, the figures showing the results are indicated. Results of data analysis from vibrometers 1, 3, 5, and 7 and pressure transducers 9 and 13 covering the time 0.2 to 1.0 second after ignition, henceforth referred to as burn time, are shown as power spectral density in figure 8, autocorrelation function in figure 9, and amplitude histogram in figure 10. Results of data analysis from vibrometers 1, 3, 5, and 7 and pressure transducers 11 and 13

covering burn time 1.4 to 2.2 seconds are shown as power spectral density in figure 11, autocorrelation function in figure 12, and amplitude histogram in figure 13.

Presented in table III are the correlation function coefficients for several combinations of transducers analyzed in the octave bandwidths of 250 to 500 Hz, 500 to 1000 Hz, 1 to 2 kHz, and 2 to 4 kHz for burn time 1.2 to 2.2 seconds and a sketch of the vehicle showing the relative position of each of the transducers. A tabulation of the statistical parameters used in this analysis is presented also.

Results from a power spectral analysis of data covering burn times 0.3 to 0.7 second and 0.7 to 1.1 seconds from vibrometers 1, 3, 5, and 7 and pressure transducer 13 are presented in figure 14.

It should be noted the ordinate scales on both the power spectral density plots and the autocorrelation function plots are set by the calibrate factor for each transducer and the analysis time period and are, thereby, unique to each plot.

Thrust and Static Pressure

Total burn time of the rocket was 3.6 seconds. The maximum thrust level, 207 kN (46 500 lb), occurred just before the decay of the thrusting period, about burn time 2.4 seconds (fig. 7). The minimum value of thrust before decay is 189 kN (42 500 lb), about burn time 0.6 second. The oscillation at the beginning of the force trace is believed to be a reaction of the support structure to the initial impulse and not a variation in the thrust since there is no indication of this oscillation in the pressure trace. The chamber pressure, transducer 4, reached a maximum value of 7.267 MN/m² (1054 psi) at burn time 0.2 second and a minimum value of 6.723 MN/m² (975 psi) at burn time 0.6 second. The trends of thrust and chamber pressure traces are generally similar.

Dynamic-Data Analysis

Fluctuating pressures.- The traces shown in figure 7 from the two pressure transducers at the forward end of the rocket motor and the one pressure transducer at the nozzle end of the rocket motor were from signals filtered by using a 10-Hz high-pass filter. Therefore, the trace shows a zero deflection when a change in the static pressure causes the instrumentation system to exceed its capabilities. This situation may be observed in the output of pressure transducer 11 from 0.1 to 0.6 second, the output of pressure transducers 11 and 13 from about 2.6 seconds to the end of the firing, and the output of pressure transducer 9 from about 1.4 seconds to the end of the firing.

During burn time 0.2 to 1.0 second, the recorded pressure oscillations were considerably higher than during the later analysis time period. Power spectral analysis of pressure transducer 9 data (fig. 8) shows maximum responses of 1.1×10^5 (N/m²)²/Hz (2.3×10^{-3} (psi)²/Hz) in the 0 to 1.8 kHz range and the 12 to 12.4 kHz range. Power

spectral analysis of pressure transducer 13 data (fig. 8) shows a maximum response of $2 \times 10^4 \text{ (N/m}^2\text{)}^2/\text{Hz}$ ($4 \times 10^{-4} \text{ (psi)}^2/\text{Hz}$) in the 10 to 10.4 kHz range with a secondary peak of $3.2 \times 10^3 \text{ (N/m}^2\text{)}^2/\text{Hz}$ ($6.8 \times 10^{-5} \text{ (psi)}^2/\text{Hz}$) in the 1.2 to 1.6 kHz range. The autocorrelation function for pressure transducer 9 (fig. 9) indicates an rms pressure of 32 kN/m^2 (4.6 psi), $\sigma_x = R_x(0)$, and the amplitude histogram (fig. 10) shows the pressure amplitudes to be approximately normally distributed. The autocorrelation function for pressure transducer 13 (fig. 9) indicates an rms pressure of 9.5 kN/m^2 (1.4 psi) and the amplitude histogram (fig. 10) shows the pressure amplitudes to be approximately normally distributed.

Interpretation of the measurements from pressure transducer 9 must include two considerations. First, a significant number of the amplitudes exceeded the linear calibrated range of $\pm 33.5 \text{ kN/m}^2$ ($\pm 4.86 \text{ psi}$), and second, the frequency content of the signal exceeded the linear frequency response of the transducer. Although the amplitude histogram did not show any significant effect, confidence in the measurements must be reduced considerably. The measurements from pressure transducer 13 within the linear operating range of the transducer (table I) are satisfactory; however, a significant amount of data exceeded the upper frequency limit. The value of the amplitude of these high-frequency components cannot be considered accurate measurements.

During burn time 1.4 to 2.2 seconds, data from pressure transducers 11 and 13 were primarily within the linear range of the measurement systems. Power spectral analysis of pressure transducer 11 data (fig. 11) shows a maximum response of $1.1 \times 10^3 \text{ (N/m}^2\text{)}^2/\text{Hz}$ ($2.3 \times 10^{-5} \text{ (psi)}^2/\text{Hz}$) in the 0 to 400 Hz range and again in the 1.8 to 2.2 kHz range. Power spectral analysis of transducer 13 data show a maximum of $1.7 \times 10^3 \text{ (N/m}^2\text{)}^2/\text{Hz}$ ($3.5 \times 10^{-5} \text{ (psi)}^2/\text{Hz}$) in the 0 to 400 Hz range and the next highest level about 20 dB down from the peak. The autocorrelation function for pressure transducer 11 (fig. 12) indicates an rms pressure of 1.1 kN/m^2 (0.16 psi) and the amplitude histogram (fig. 13) shows the amplitudes to be normally distributed. The autocorrelation function for pressure transducer 13 (fig. 12) indicates an rms pressure of 1.1 kN/m^2 (0.16 psi) and the amplitude histogram (fig. 13) shows the amplitudes to be normally distributed.

Filtering of the pressure oscillation signals from pressure transducer 13 during burn time 0.2 to 1.0 second with a 5-kHz low-pass filter yielded an rms pressure of 2.3 kN/m^2 (0.34 psi). Although the spectrum amplitudes are not in good agreement for the 0.2 to 1.0 second and the 1.2 to 1.4 second time periods, the root-mean-square values when filtered are of the same order of magnitude and the frequencies (i.e., 0 to 400 Hz and 1.0 to 1.6 kHz) at which peaks are observed are common to both spectrum shapes.

Fluctuating vibrations. - The vibration levels observed during burn time 0.0 to 1.2 seconds are considerably higher than those observed from 1.2 seconds to burnout

(fig. 7). Although this rocket support and test system are considerably different from that used in reference 5, the higher vibratory levels were in the same frequency range of 10 kHz as was observed in reference 5. The maximum power spectral level occurred on vibrometer 1, which is mounted directly behind pressure transducer 9, and reached $0.21 \text{ g}^2/\text{Hz}$ in the 10 to 10.4 kHz range (fig. 8). During the analysis time period 1.4 to 2.2 seconds the highest power spectrum level is also on vibrometer 1 and reaches a peak value of $0.12 \text{ g}^2/\text{Hz}$ at 1.9 kHz (fig. 11). The amplitude histograms for the two time segments analyzed (figs. 10 and 13) indicate a normal distribution for all the measurements with peak values generally three to four times the root-mean-square values. The maximum level of vibration observed, $31.5g_{\text{rms}}$, was on the nozzle end of the vehicle during burn time 0.2 to 1.0 second. This level of vibration dropped to $7.4g_{\text{rms}}$, with the disappearance of the high-frequency components, during burn time 1.4 to 2.2 seconds.

Correlation function coefficient.- The maximum correlation function coefficient was determined, by using equation (2), for several combinations of measurements (table III). In the bandwidth 250 to 500 Hz, correlation coefficients of 0.84 between vibrometers 5 and 7 and 0.51 between vibrometers 3 and 5 indicate a strong vibration interaction at these locations. Such interaction indicates that the vibration at these locations is related by a linear transfer function. The longitudinal modes of a linear system would represent such a transfer function.

The coefficient between the vibrometers decreases with increasing frequency which indicates that the motion at these locations is less dependent on the vehicle modes and is related more to the local conditions. The coefficient between vibrometers 3 and 5 has dropped to 0.35 in the bandwidth 500 to 1000 Hz, whereas between vibrometers 5 and 7, which are physically closer together than vibrometers 3 and 5, the coefficient is still a relatively high value of 0.69. Analysis at the higher frequencies, 2 to 4 kHz, continues to show the trend of the reduced correlation with the value of 0.13 between vibrometers 3 and 5, a value indicating almost complete independence or a nonlinear relationship.

Since the measurements from pressure transducer 13 and vibrometer 7 were made at the same location, the relatively low correlation function coefficient throughout the frequency range of analysis was not expected. However, a post-test calibration of the pressure transducer in its mounting indicated that the phase response varied slightly with frequency when compared to an accelerometer. This could account for the low correlation function coefficient.

A relatively high correlation coefficient of 0.54 was calculated between pressure transducers 11 and 13 in the 250 to 500 Hz range. However, the value of 0.32 in the 500 to 1000 Hz range and 0.32 in the 2 to 4 kHz range is in an uncertain area of interpretation. The value of 0.49 in the 1 to 2 Hz range is a fair to good degree of correlation. The apparent frequency dependency of correlation may be explained by inspecting the power-

spectral-density plots for these transducers (fig. 11). The pressure spectrum drops noticeably in the 500 to 1000 Hz range and then increases in the 1 to 2 kHz range only to fall off again in the 2 to 4 kHz range. The low values of the coefficient may be due to the lower values of pressure being affected by uncorrelated background noise of the system whereas the higher pressure levels are less affected. These data would suggest that the pressure spectrum across the dome is relatively well correlated over the analyzed frequency range.

High-Frequency-Data Analysis

A power spectral analysis of the high-frequency vibrations that occur during the first 1.2 seconds of burn time was conducted by dividing this time period into two segments, 0.3 to 0.7 second and 0.7 to 1.1 seconds. The bandwidth of analysis was 80 Hz, twice that used in the prior analysis. Since the time increment of analysis is halved and the bandwidth is doubled, the confidence level is the same for this spectral analysis as it is for the earlier analysis. A comparison of the frequency spectrum for vibrometers 1, 3, 5, and 7 during the two time periods (fig. 14) shows that the low-frequency vibration (i.e., 0 to 8 kHz) remains relatively the same. The spectrum during burn time 0.3 to 0.7 second has significant response in the 12 to 14 kHz range for all the vibrometers; however, this response disappears during burn time 0.7 to 1.1 seconds. Although vibrometers 5 and 7 do not show an increase in response in the 10 to 12 kHz range, vibrometers 1 and 3 do show such an increase at these lower frequencies at the later burn time. Investigation of measurements from pressure transducer 13 yields results similar to those for measurements from vibrometers 1 and 3, that is, no change in the spectrum at the lower frequencies and the maximum response (during burn time 0.3 to 1.1 seconds) decreases from a frequency range of 12 to 14 kHz to 10 to 12 kHz. Since the measurements from pressure transducer 9 severely overdrove the system, it was not investigated further. This reduction of the frequencies of major input indicates that the source of this vibration is changing. A possible explanation for the source of this vibration is that the lateral slots in the grain form an acoustic chamber which, as the grain burns, increase in size and reduce the frequency of the chamber. This would not explain the sharp disappearance of the vibration. However, by using the formula

$$f = \frac{\sqrt{\gamma g R T_1}}{\lambda}$$

where

f frequency, Hz

γ specific heat ratio

g	acceleration of gravity
R	gas constant
T ₁	absolute temperature
λ	wavelength

and any consistent set of units, frequencies in the range of 12 to 14 kHz at a temperature of 2478 K (4000° F) would develop in a chamber approximately 8.6 cm (3.4 inches) long. The long dimension of the inside slot in the grain is 9.1 cm (3.6 inches). In addition, as the grain burns, the slot dimension increases and causes the resonant frequency of the gaseous medium in the slot opening to decrease. Although this explanation does not prove that the high frequencies are generated in the slots in the grain, it does indicate that these frequencies could be a function of the grain geometry.

CONCLUDING REMARKS

A Nike rocket motor, instrumented to obtain dynamic measurements, was fired against a backstop. The rocket reached a maximum thrust of 207 kN (46 500 lb) and burned for 3.6 seconds.

Root-mean-square pressure oscillations in the rocket chamber, on top of the static pressure of 7.267 MN/m² (1054 psi), reached a maximum value of 32 kN/m² (4.6 psi) at the nozzle end of the rocket and 9.5 kN/m² (1.4 psi) at the forward dome. These maximum oscillations occurred during the first 1.2 seconds of burning and included significant components in the 10 to 12.4 kHz frequency range. The high-frequency components disappeared after 1.2 seconds of burning time and the rms pressure oscillations at the forward dome dropped to 1.1 kN/m² (0.16 psi). If initial pressure data are filtered to allow only the frequency components below 5 kHz to be analyzed, the rms pressure oscillation at the forward dome is 2.3 kN/m² (0.34 psi).

The vibrations developed from the pressure oscillations yielded a similar frequency spectrum (i.e., high response in the 10 to 12.4 kHz range which disappeared after the first 1.2 seconds of burning). The vibration reached levels as high as 31.5g_{rms} during the first 1.2 seconds but in the absence of the high-frequency components dropped to 7.4g_{rms}. Although no explanation for the disappearance of these high-frequency components was determined, it appears that these frequencies are associated with the geometry of the grain used in the Nike rocket.

Statistical analysis of the random data indicated that the responses follow a normal distribution with peak values generally three to four times the root-mean-square values.

Relatively high values of the correlation coefficient for the vibrometers at frequencies below 500 Hz indicate that the motion is primarily dependent on the longitudinal modes of the total vehicle. As the frequency increases the correlation coefficient decreases until, in the frequency range from 2 to 4 kHz, the vibration of the structure is relatively independent of linear modes of the total vehicle and depends primarily on the local structural characteristics.

Similar correlation studies of the oscillations at two locations on the forward dome indicate that the pressures on the dome are relatively well correlated over the range of 0.25 to 4 kHz.

Langley Research Center

National Aeronautics and Space Administration,
Hampton, Va., October 12, 1972.

REFERENCES

1. Achenbach, J. D.: The Structural Dynamics of Solid Propellant Rockets. *Appl. Mech. Rev.*, vol. 21, no. 6, June 1968, pp. 549-555.
2. Baltrukonis, J. H.: A Survey of Structural Dynamics of Solid Propellant Rocket Motors. NASA CR-658, 1966.
3. Meirovitch, Leonard; and Wesley, Donald A.: On the Dynamic Characteristics of a Variable-Mass Slender Elastic Body Under High Accelerations. NASA CR-713, 1967.
4. Meirovitch, Leonard: The General Motion of a Variable-Mass Flexible Rocket With Internal Flow. NASA CR-1528, 1970.
5. Schoenster, James A.: Measurements and Analysis of Solid-Propellant-Rocket Vibrations Obtained During a Captive Flight. NASA TN D-6517, 1971.
6. Clevenson, Sherman A.: Payload Vibration Data Measured During Five Flights of a Two-Stage Solid-Propellant Launch Vehicle. NASA TN D-963, 1962.
7. Manning, James C.: Some Flight-Induced Environmental Data Obtained From Two Sidewinder-Arcas Sounding-Rocket Launches. NASA TM X-2368, 1971.
8. Fowler, J. R.; and Rosenthal, J. S.: Missile Vibration Environment for Solid Propellant Oscillatory Burning. AIAA Paper No. 71-756, June 1971.
9. Bergman, G. H.; and Jessen, E. C.: Evaluation of Conventional Rocket Motor Instrumentation for Analysis of Oscillatory Combustion. AIAA Paper No. 71-755, June 1971.
10. Pendleton, Lane R.: Sinusoidal Vibration of Poseidon Solid Propellant Motors. *Shock & Vib. Bull.*, Bull. 42, Pt. 3, U.S. Dep. Def., Jan. 1972, pp. 89-98.
11. Bendat, Julius S.; and Piersol, Allan G.: *Measurement and Analysis of Random Data*. John Wiley & Sons, Inc., c.1966.
12. White, Pritchard H.: *Cross-Correlation in Structural Vibration*. MEL Rep. 510/66, U.S. Navy, July 31, 1966. (Available from DDC as AD 648 359.)

TABLE I.- OPERATING RANGE AND CALIBRATIONS FOR THE DATA MEASURING SYSTEMS

[For instruments as mounted]

Instrument	Linear operating range		Calibrate signal	
	Amplitude	Frequency, Hz	Amplitude	Frequency, Hz
Vibrometer 1	±118g	3 to 5000	±100g	1000
Vibrometer 3	±107g	3 to 5000	±100g	1000
Vibrometer 5	±109g	3 to 5000	±100g	1000
Vibrometer 7	±113g	3 to 5000	±100g	1000
Pressure transducer 4	10.32 MN/m ² (1500 psi)	0 to 50	6.73 MN/m ² (976 psi)	dc
Pressure transducer 9	±33.5 kN/m ² (±4.86 psi)	20 to 2500	±16.75 kN/m ² (±2.43 psi)	1000
Pressure transducer 11	±31.5 kN/m ² (±4.58 psi)	20 to 5000	±15.79 kN/m ² (±2.29 psi)	1000
Pressure transducer 13	±32.5 kN/m ² (±4.72 psi)	20 to 5000	±16.27 kN/m ² (±2.36 psi)	1000
Load cell 6	282 kN (63 400 lb)	0 to 50	141 kN (31 700 lb)	dc

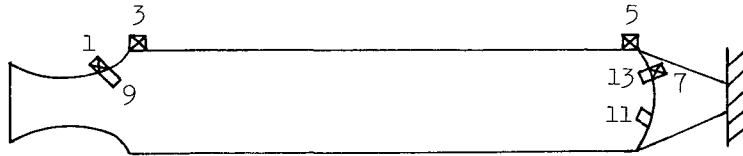
Note: The vibrometer measuring system was within 1.2 dB at 10 000 Hz.

TABLE II.- DATA-ANALYSIS ESTIMATE PARAMETERS

Parameter	Time from ignition, sec	
	0.2 to 1.0	1.4 to 2.2
Record length, sec	0.8	0.8
Power spectra:		
Frequency range, Hz	0 to 20 000	0 to 20 000
Bandwidth, B, Hz	40	40
Degrees of freedom, k	64	64
90% confidence interval, dB	±2.5	±2.5
Amplitude histogram:		
Sample interval, ϵ , μ sec	25	50
Autocorrelation function:		
Sample interval, ϵ , μ sec	25	50
Number of time lags, m	99	99
Sample size, n	32×10^3	16×10^3
Degrees of freedom, k	646	323
Bandwidth, B, Hz	401	200
90% confidence interval, dB	±0.036	±1.2

TABLE III.- CORRELATION FUNCTION COEFFICIENTS AND
STATISTICAL PARAMETERS

[Time from ignition, 1.2 to 2.2 sec]



Transducer combination	Correlation function coefficient for frequency range, Hz, of -			
	250 to 500	500 to 1000	1000 to 2000	2000 to 4000
11 and 13	0.54	0.32	0.49	0.32
7 and 13	.29	.22	.37	.30
5 and 7	.84	.69	.29	.33
3 and 5	.51	.35	.19	.13

Statistical parameter	Value of parameter for frequency range, Hz, of -			
	250 to 500	500 to 1000	1000 to 2000	2000 to 4000
Time, sec	1.0	1.0	1.0	1.0
Bandwidth, B, Hz	40	80	80	200
Degrees of freedom, k	80	160	160	320
Sample interval, ϵ , μ sec	250	125	50	12.5

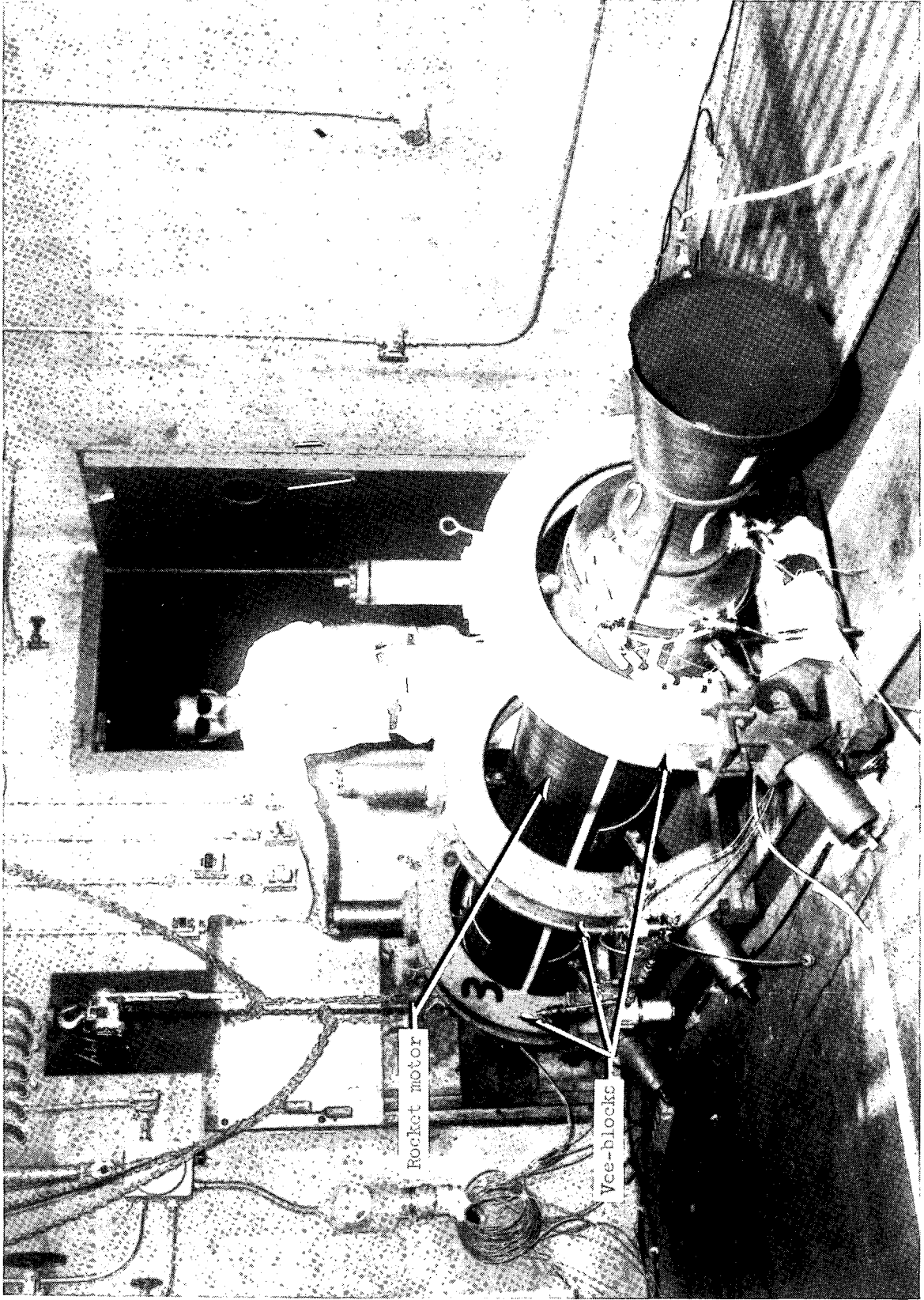
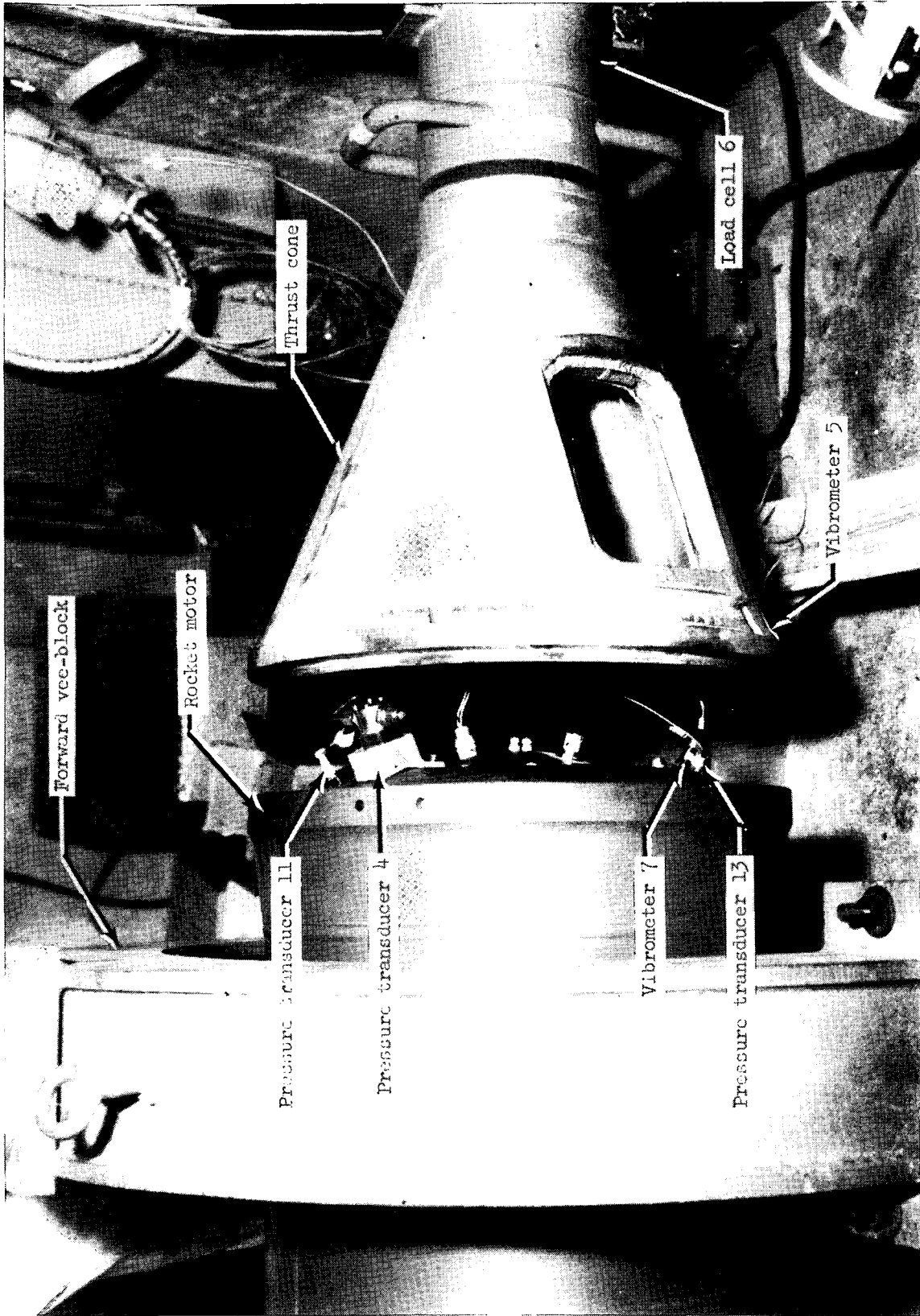


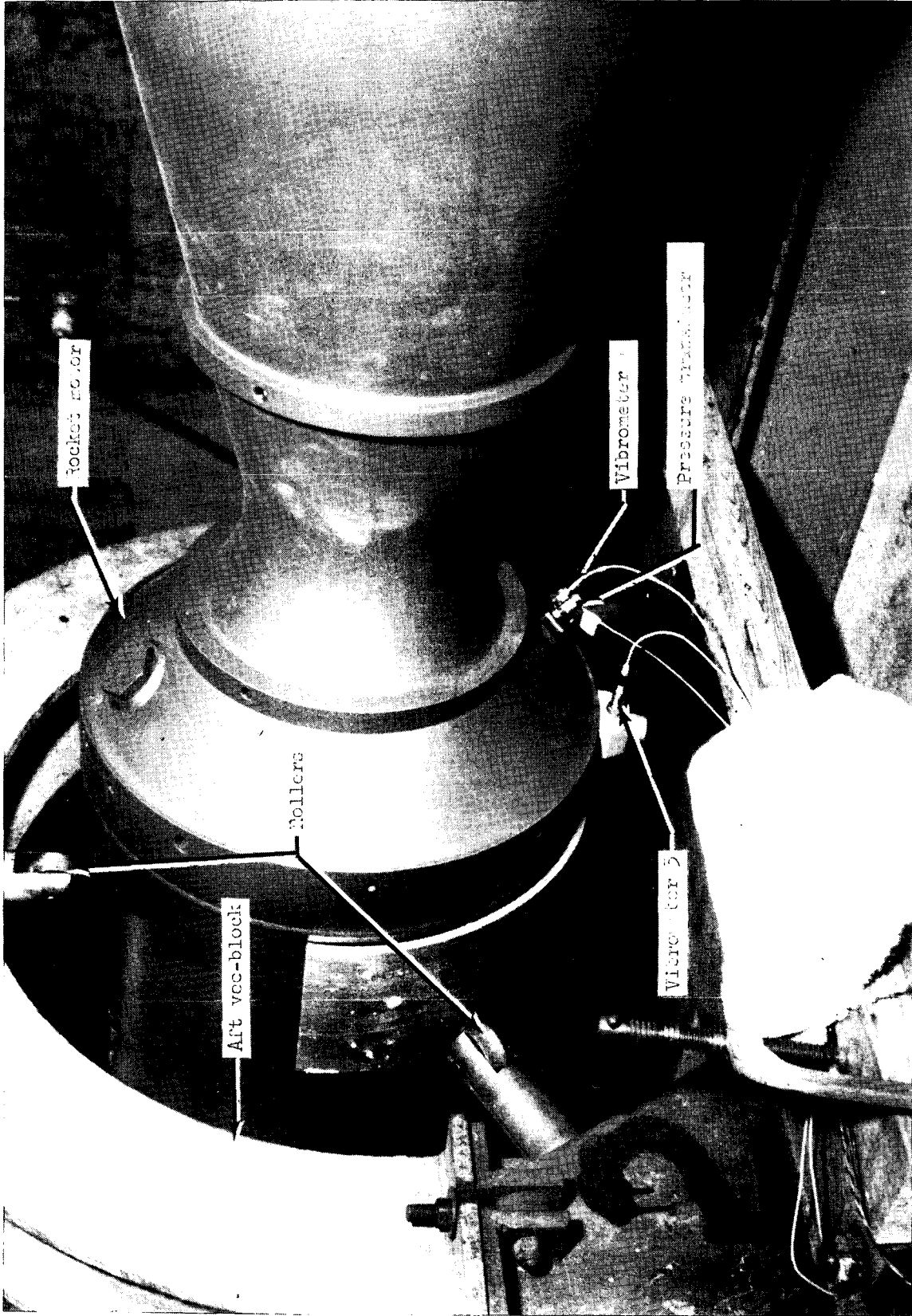
Figure 1.- Horizontal test stand.

L-71-4569.1



L-71-7017.1

Figure 2.- Forward end of rocket motor and test stand.



L-71-7021.1

Figure 3.- Aft end of rocket motor and test stand.

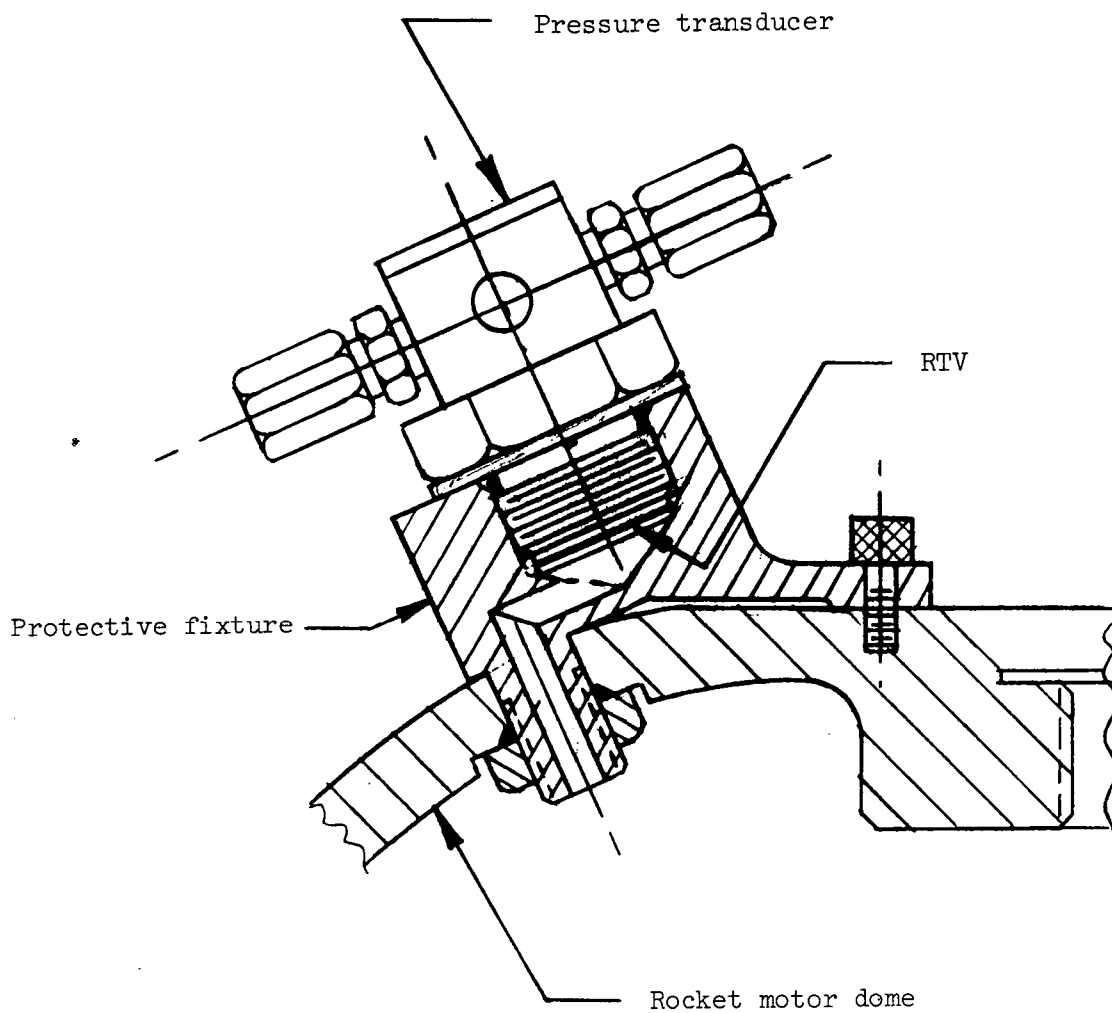


Figure 4.- Pressure transducer 4 in protective fixture
(shown approximately twice normal size).

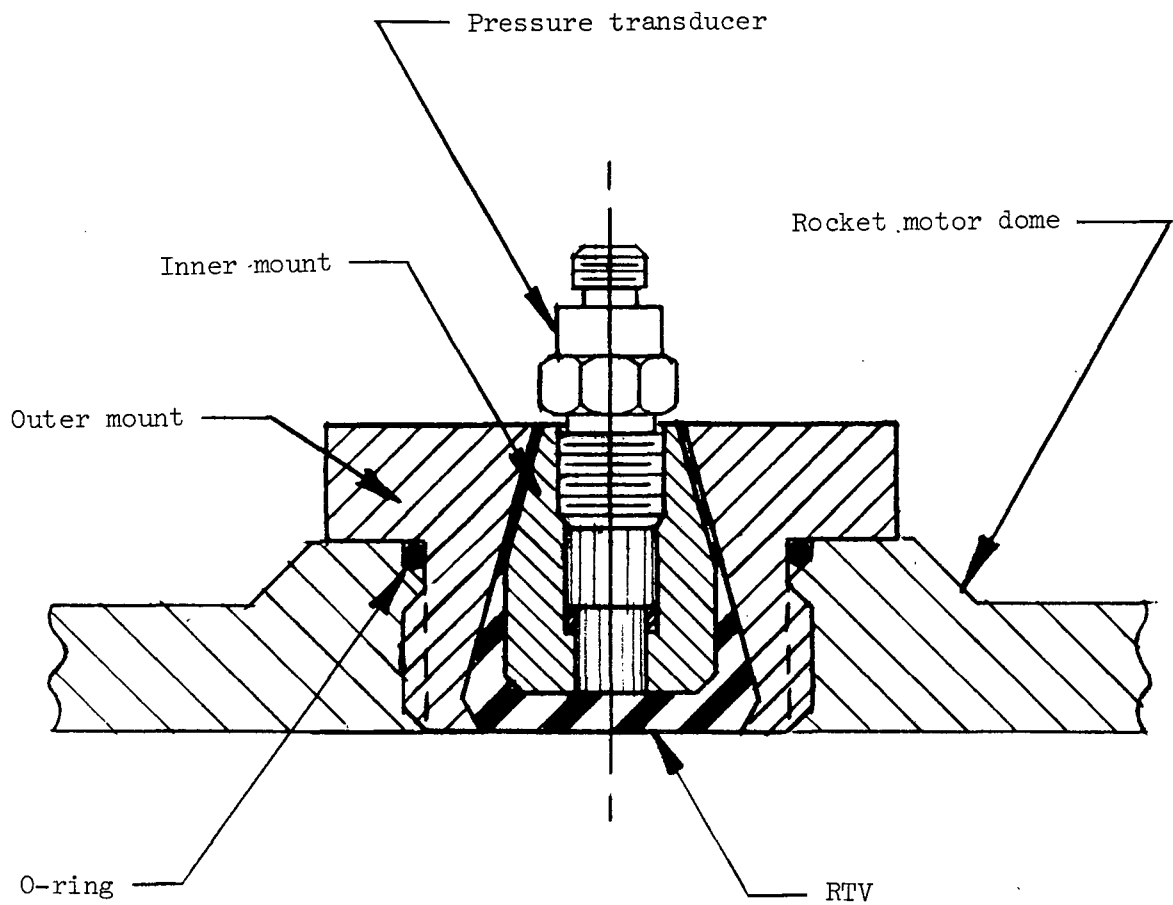


Figure 5.- Pressure transducers 11 and 13 in dome mounting
(shown approximately twice normal size).

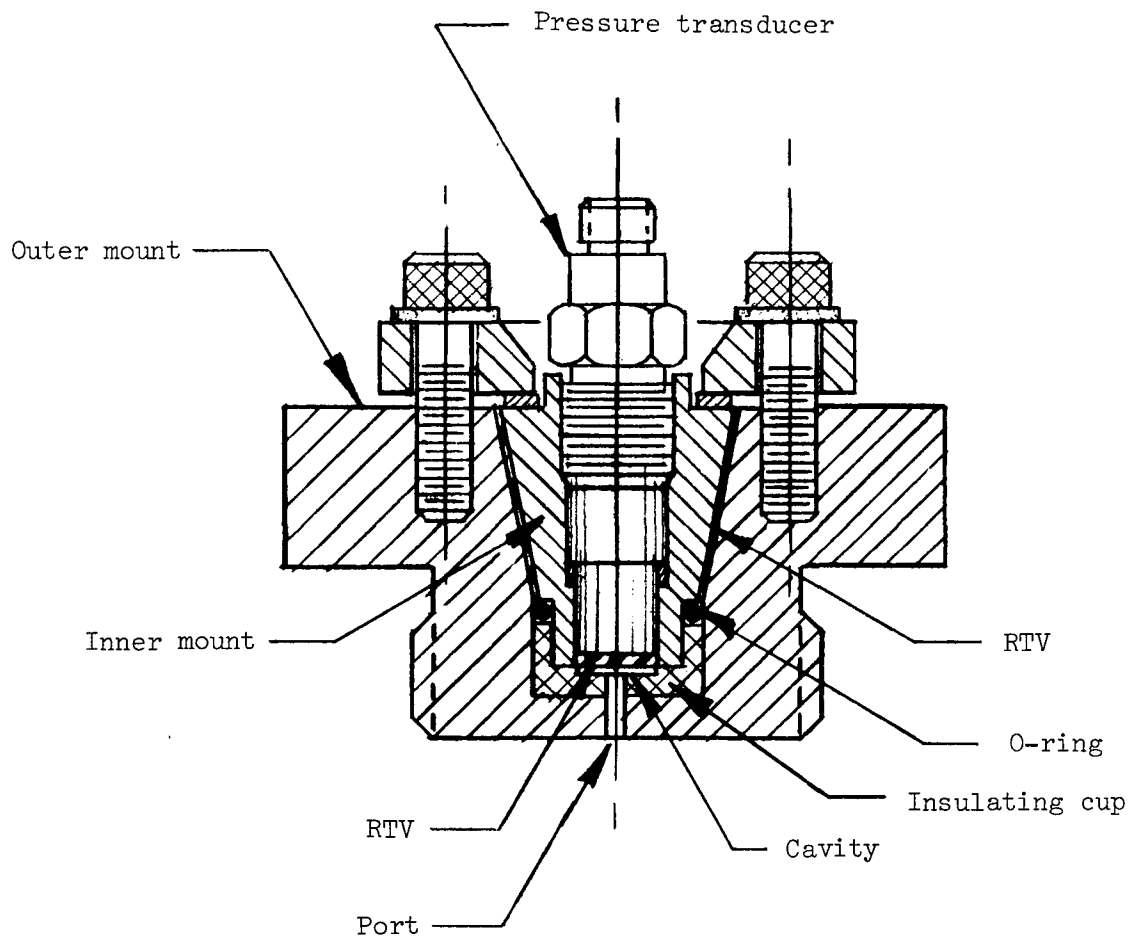


Figure 6.- Pressure transducer 9 in nozzle mounting
(shown approximately twice normal size).

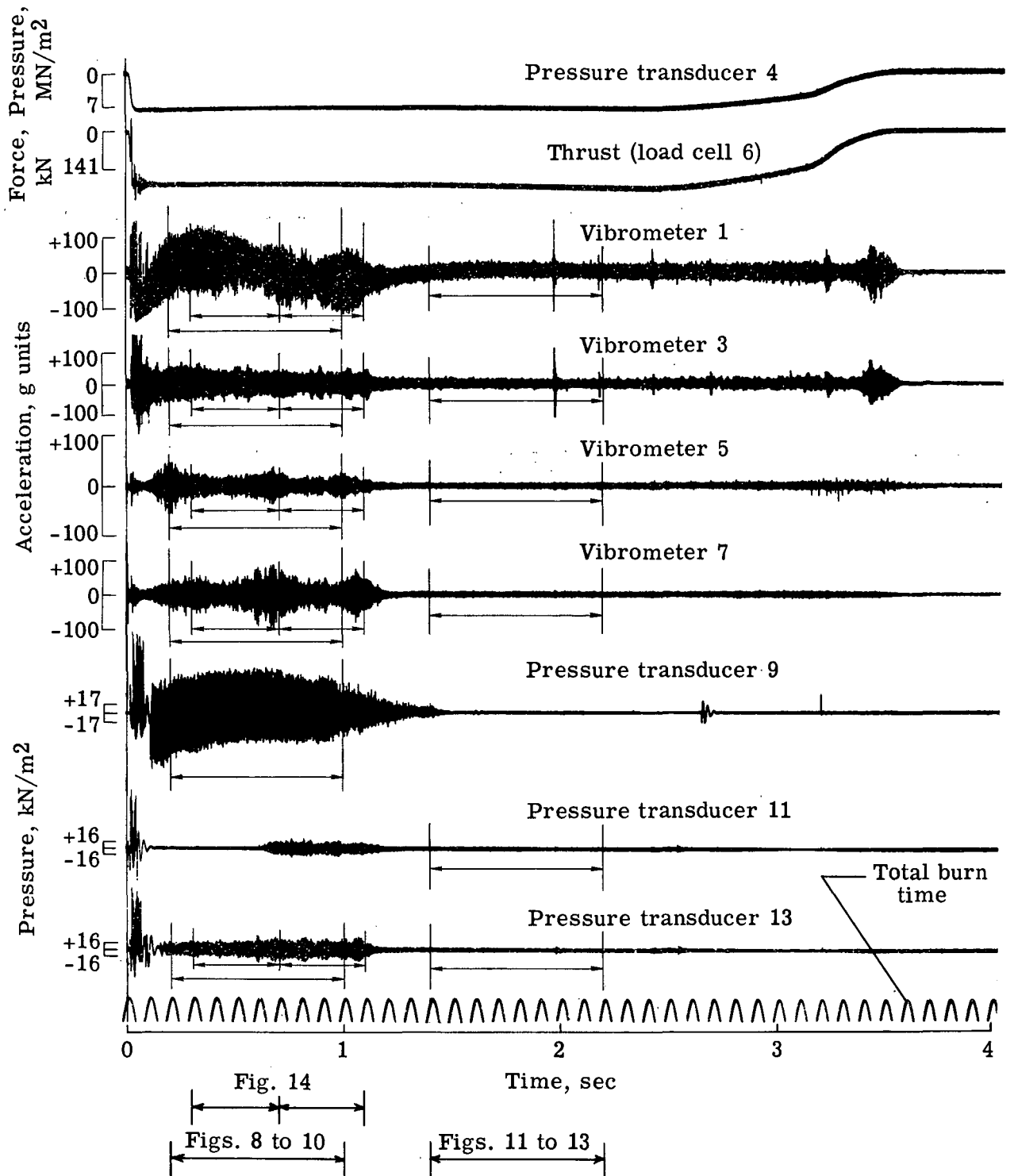


Figure 7.- Oscillograph records from Nike backstop firing. (Vertical lines show analysis times. Figures showing analysis results are listed at bottom of figure.)

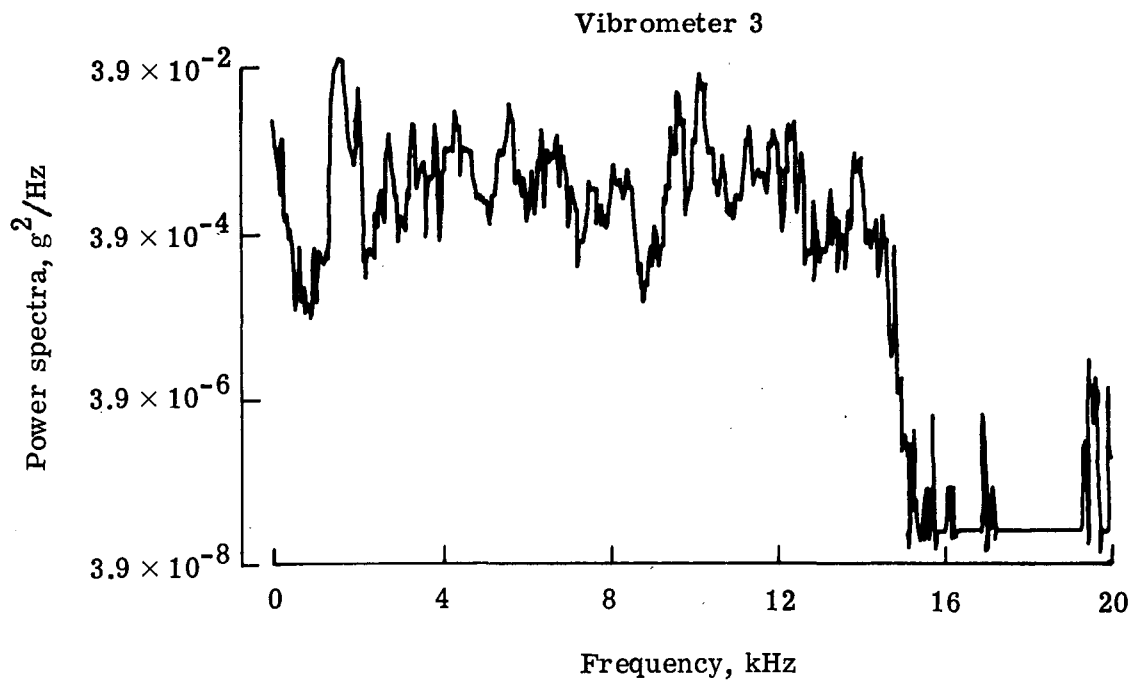
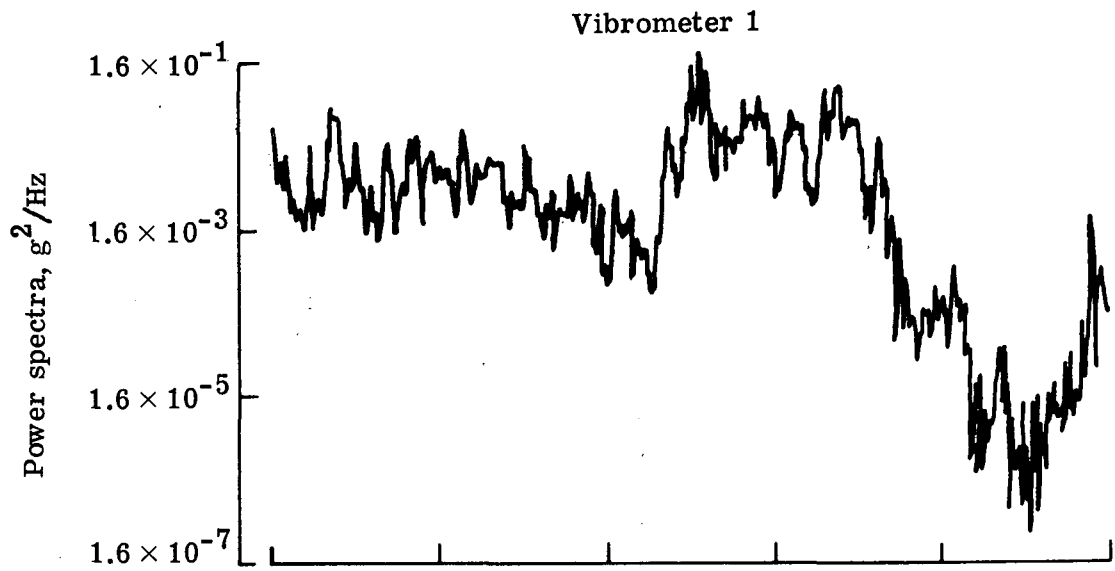
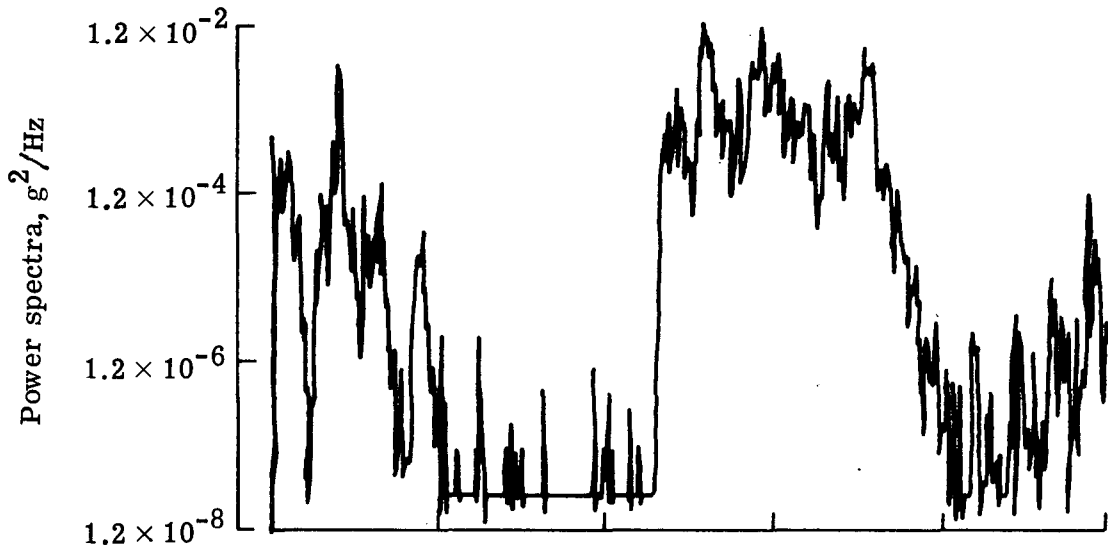


Figure 8.- Power-spectral-density measurements for burn time 0.2 to 1.0 sec.

Vibrometer 5



Vibrometer 7

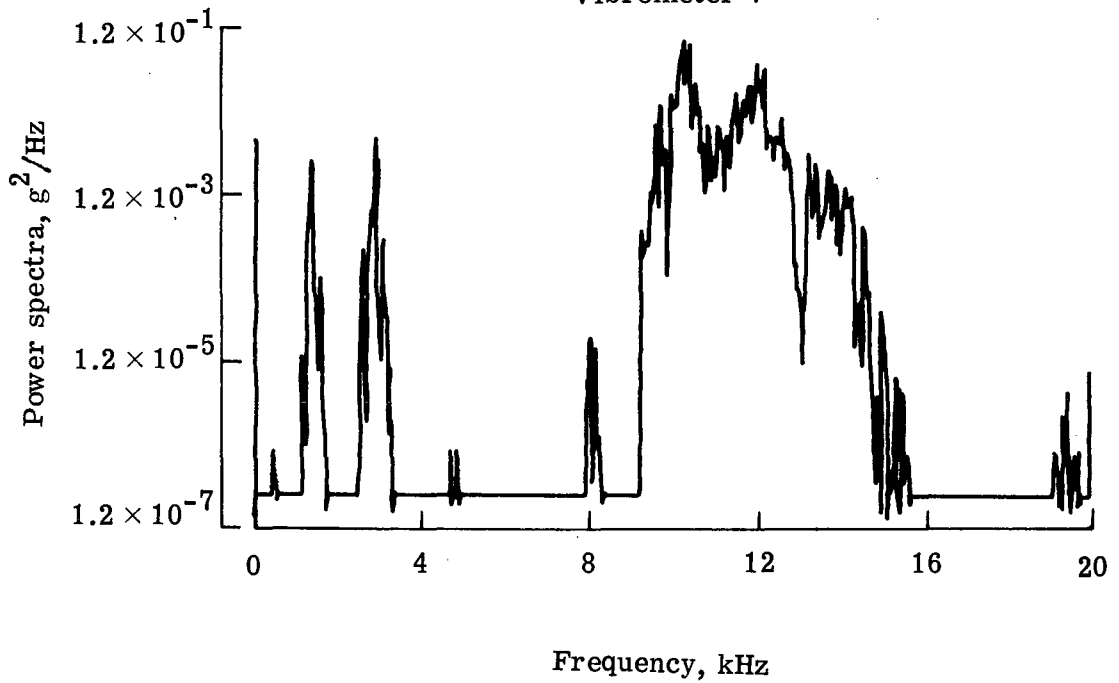


Figure 8.- Continued.

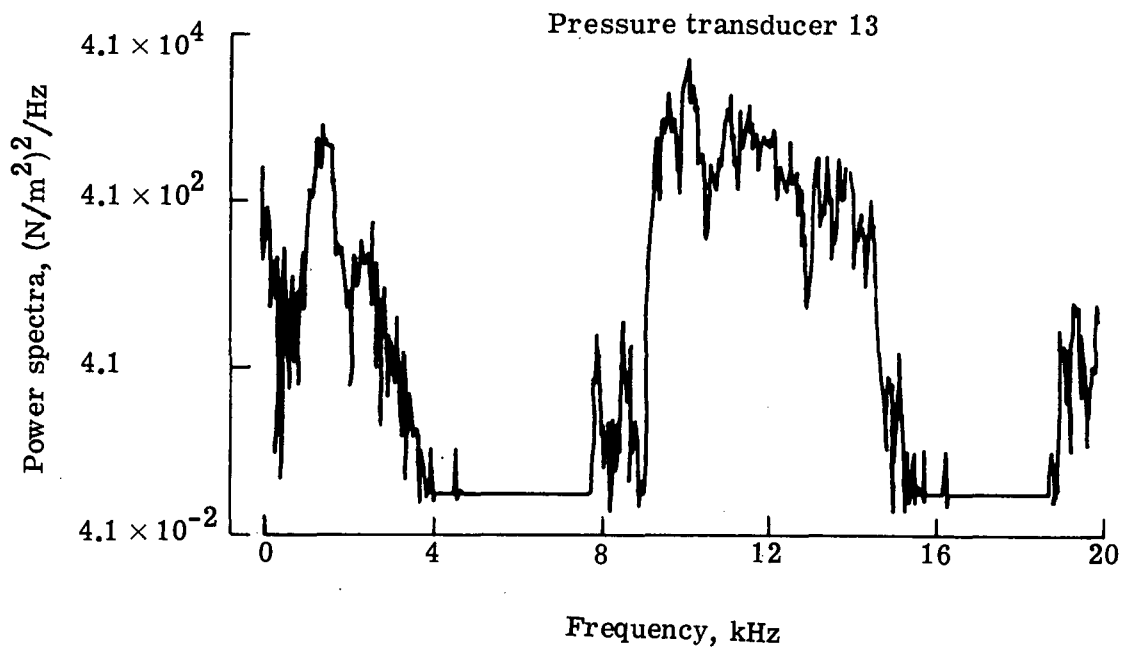
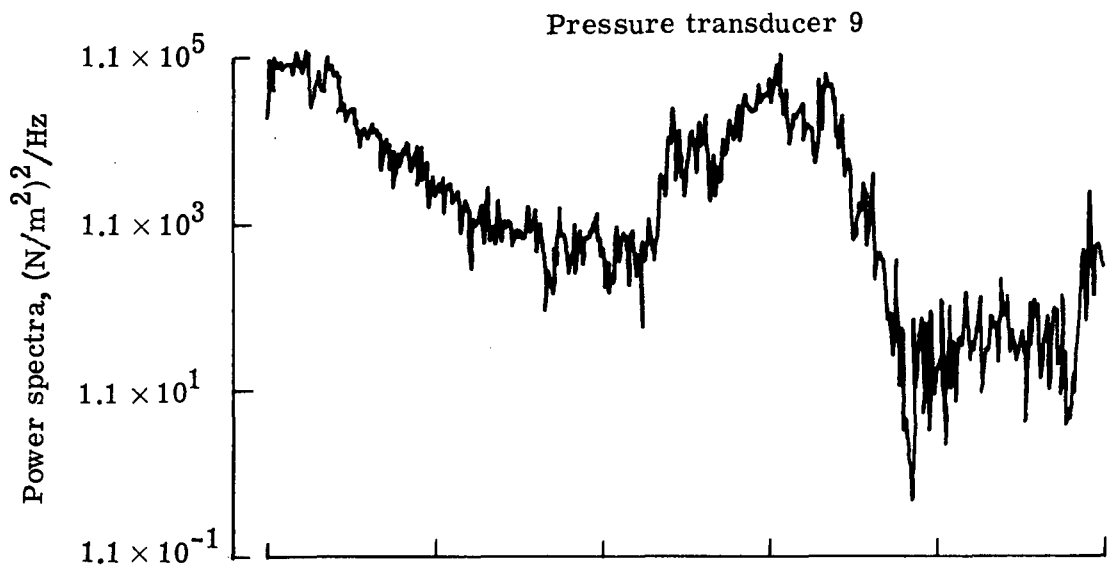


Figure 8.- Concluded.

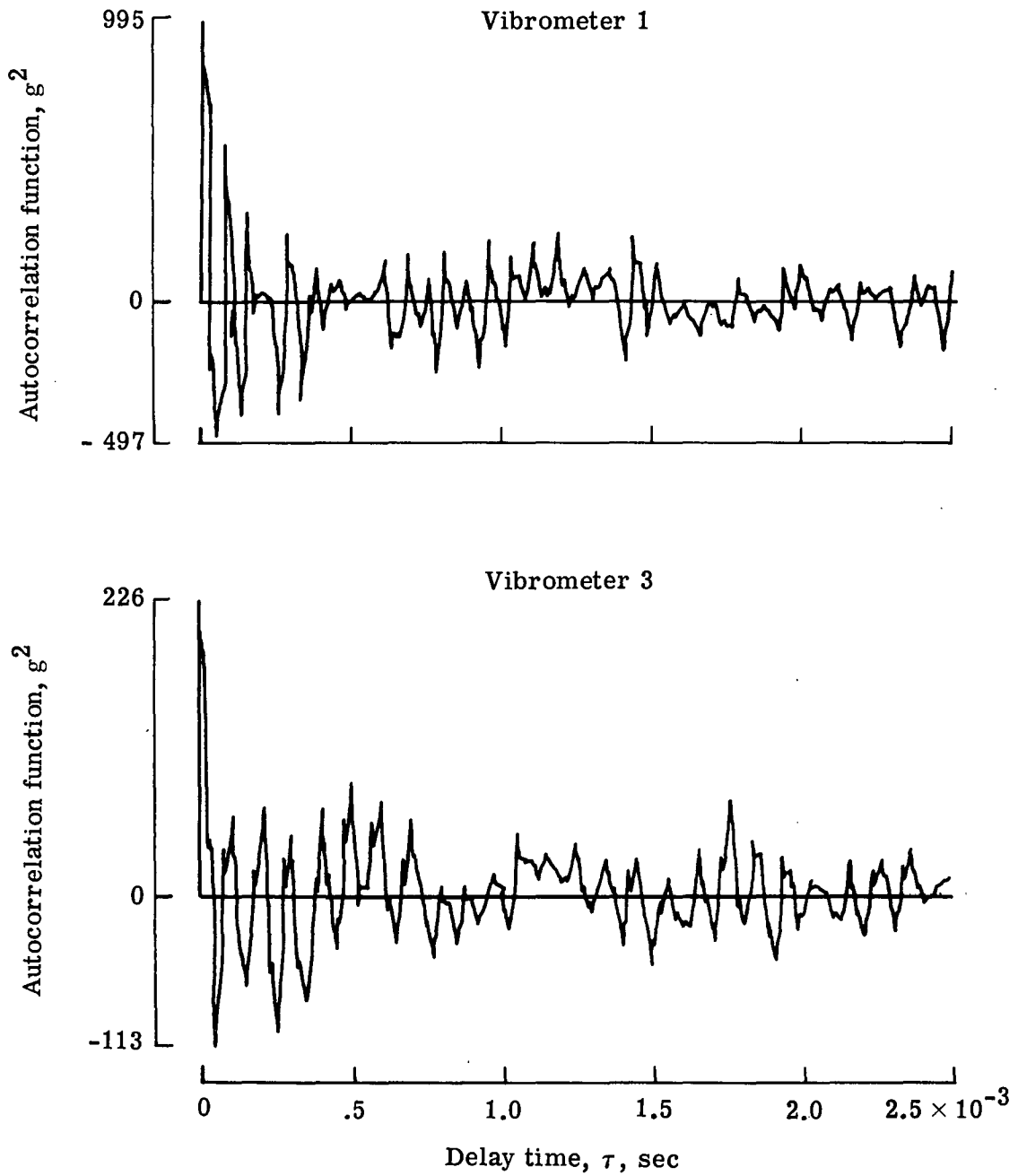


Figure 9.- Autocorrelation function for burn time 0.2 to 1.0 sec.

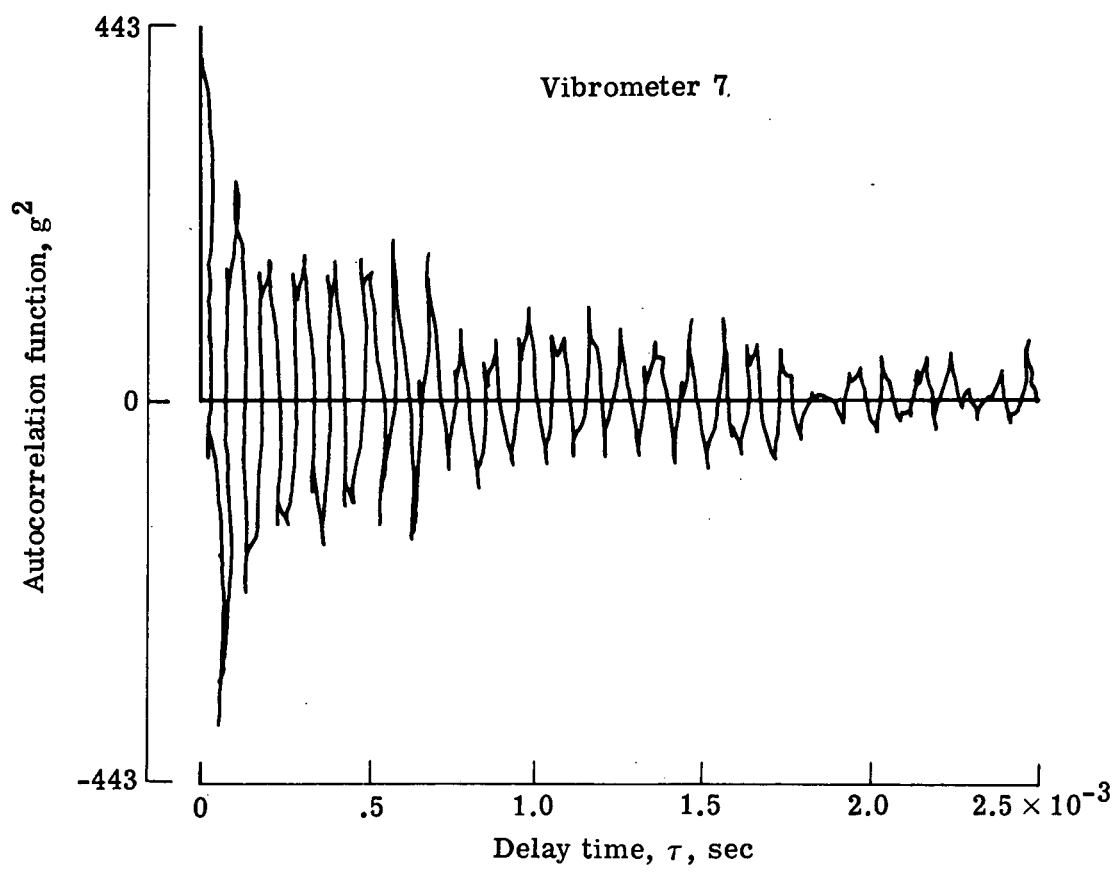
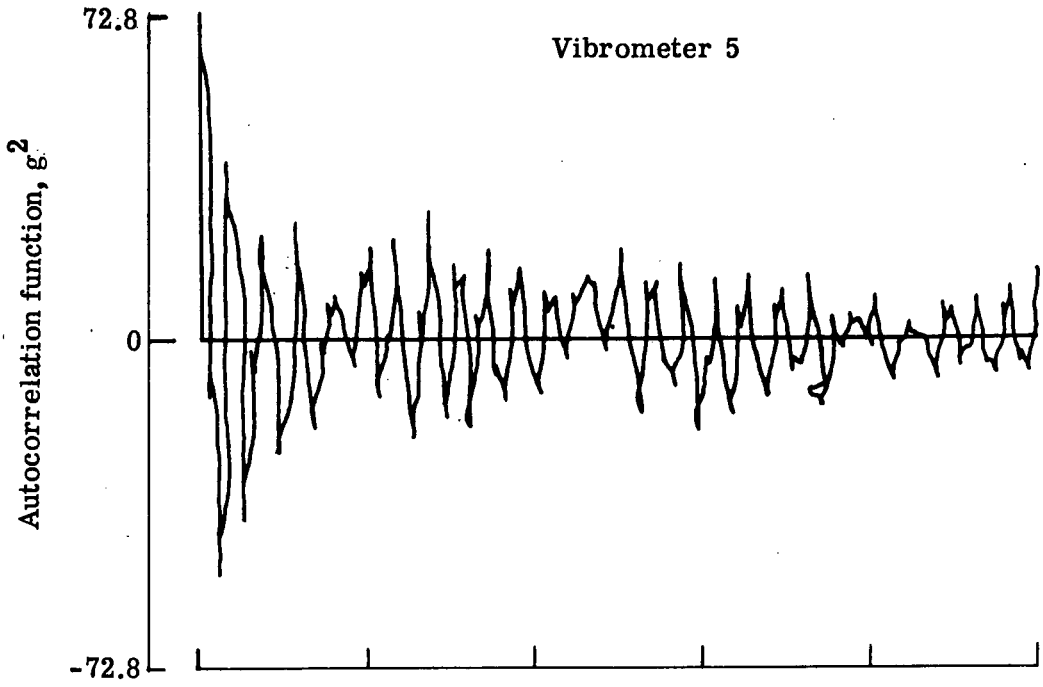


Figure 9.- Continued.

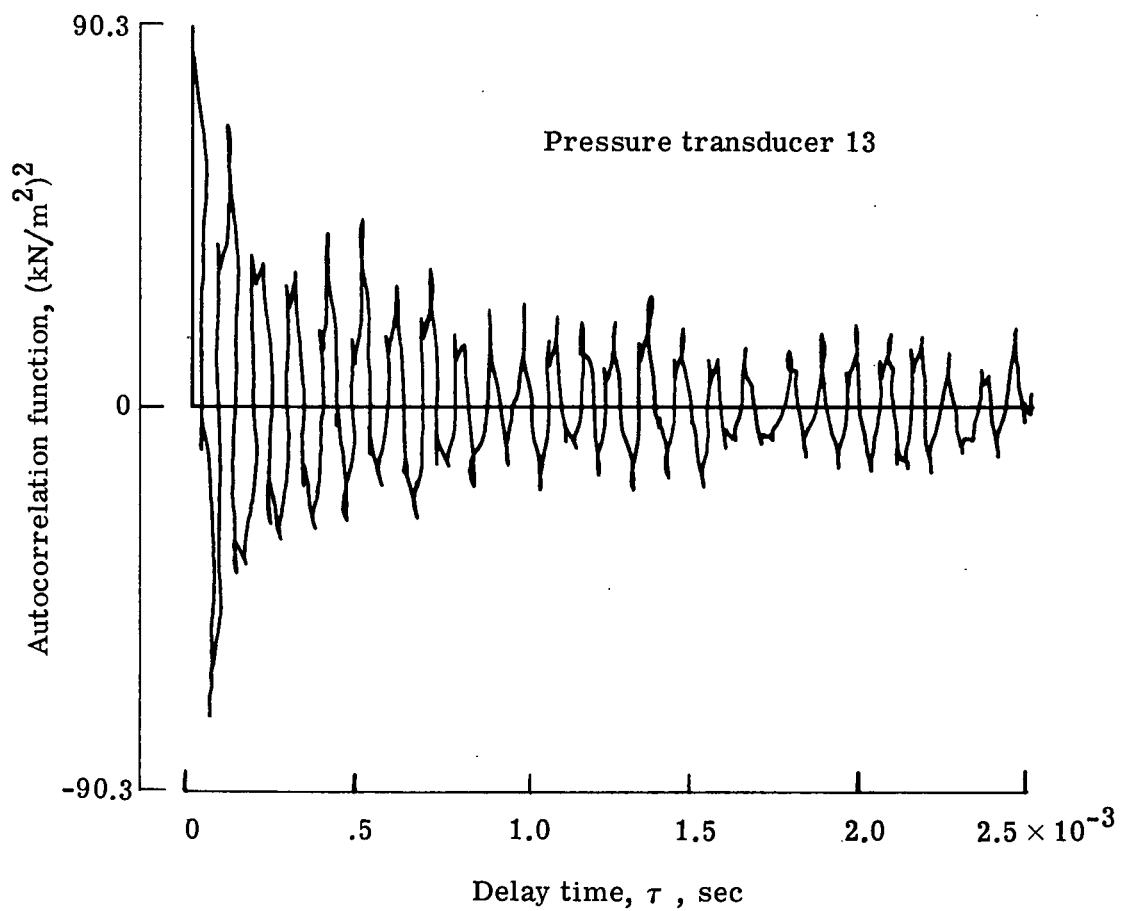
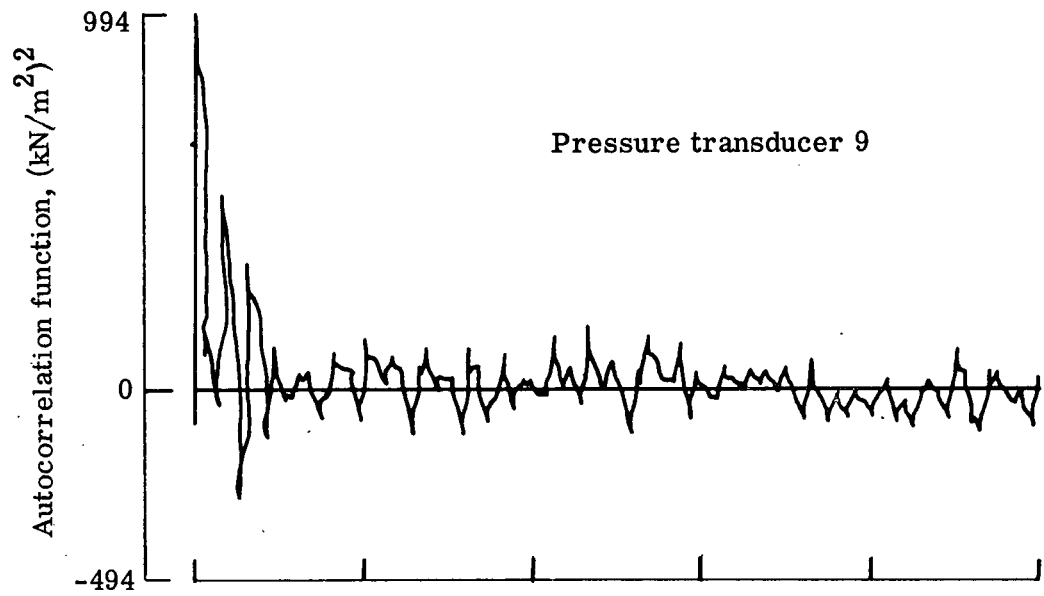


Figure 9.- Concluded.

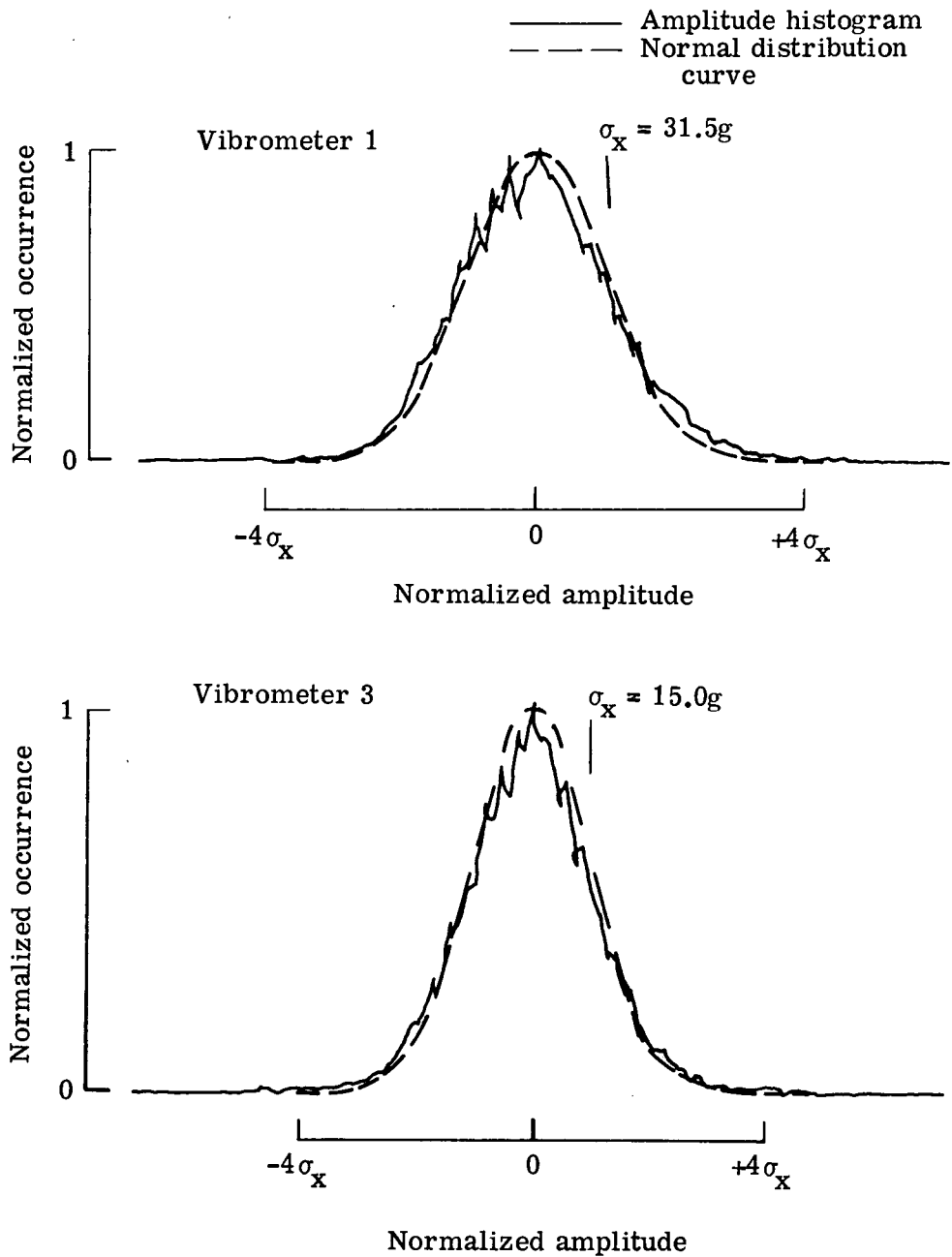


Figure 10.- Amplitude histogram for burn time 0.2 to 1.0 sec.

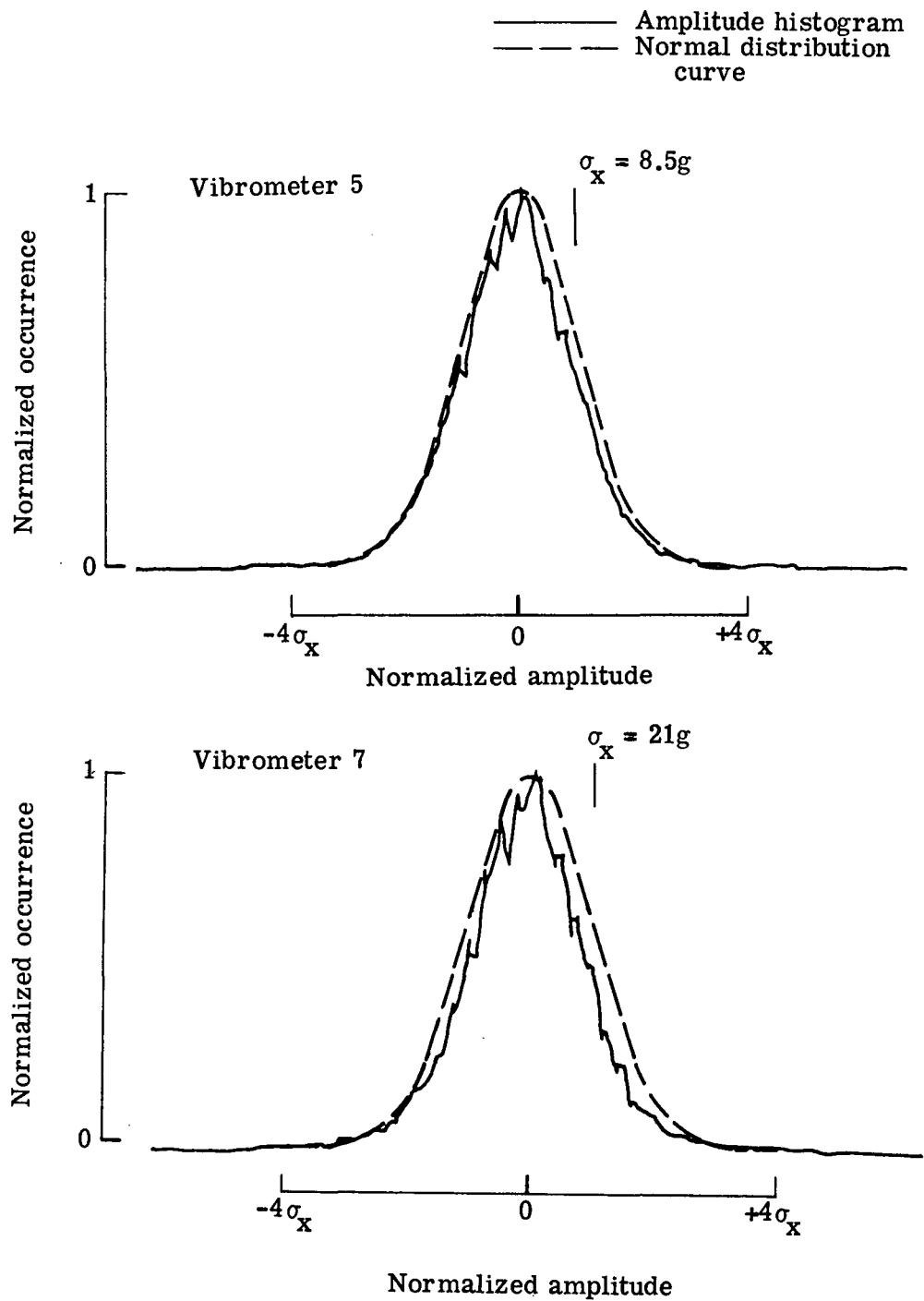


Figure 10.- Continued.

— Amplitude histogram
- - - Normal distribution curve

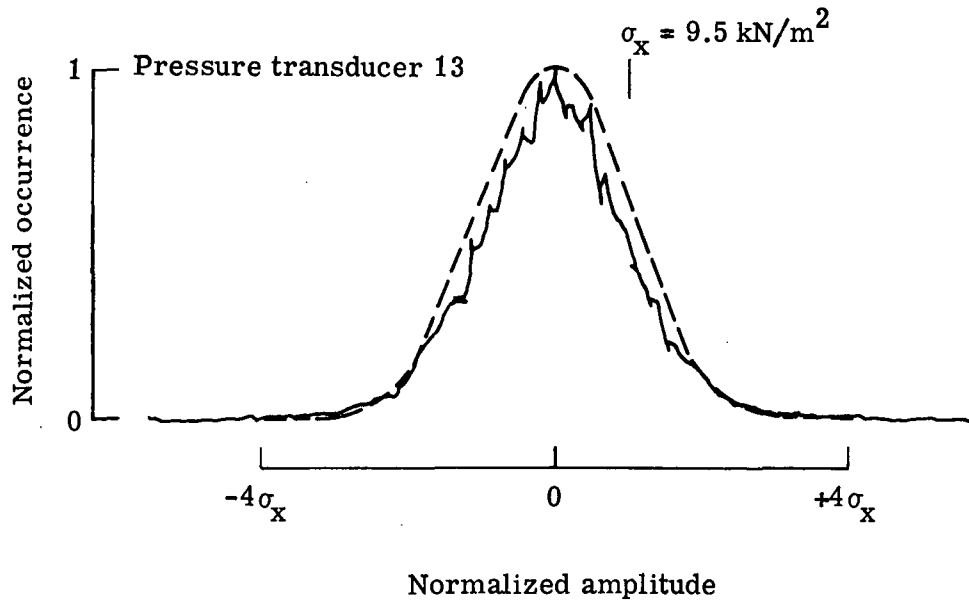
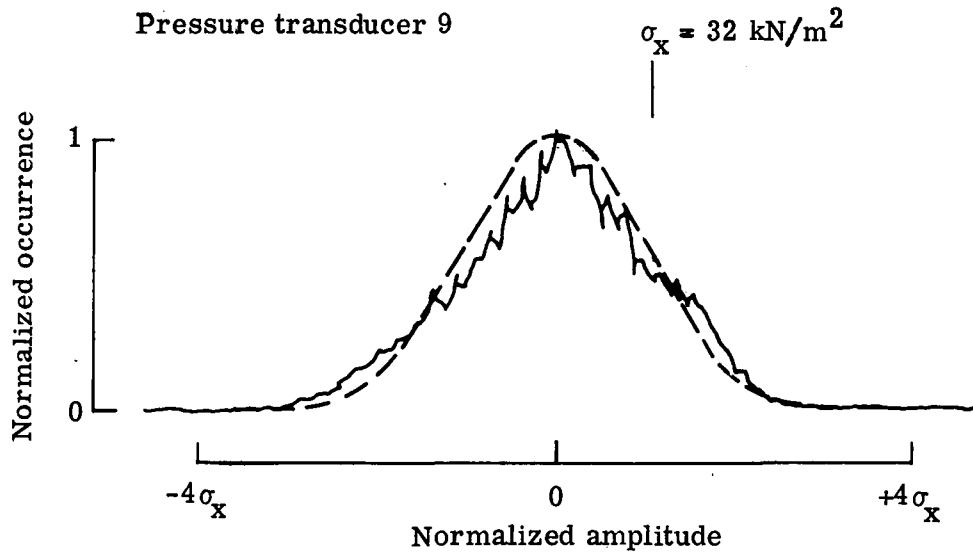


Figure 10.- Concluded.

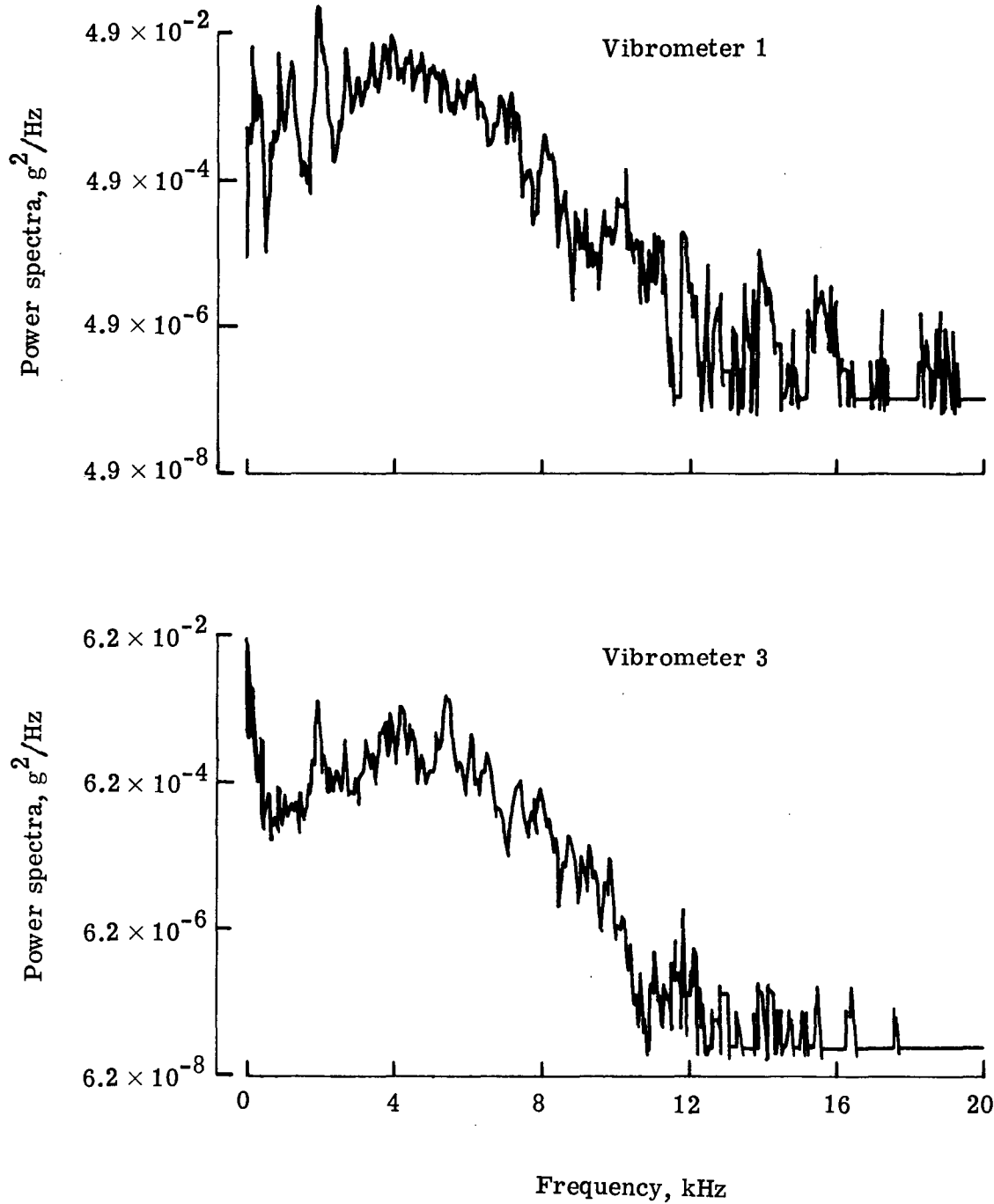


Figure 11.- Power-spectral-density measurements for burn time 1.4 to 2.2 sec.

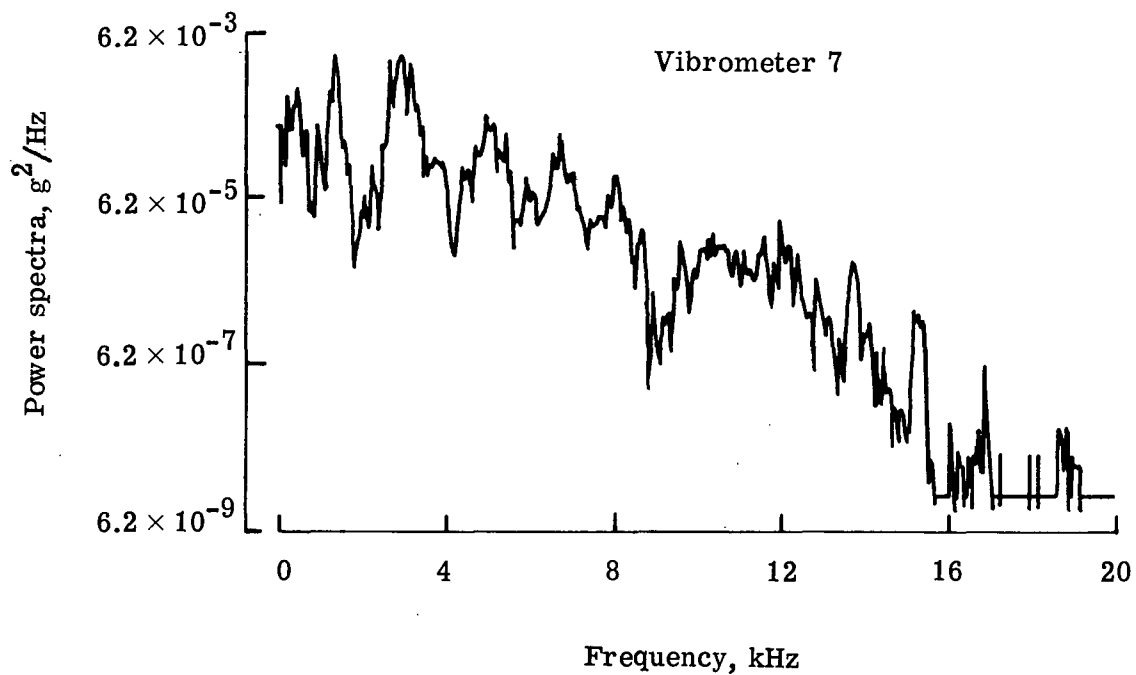
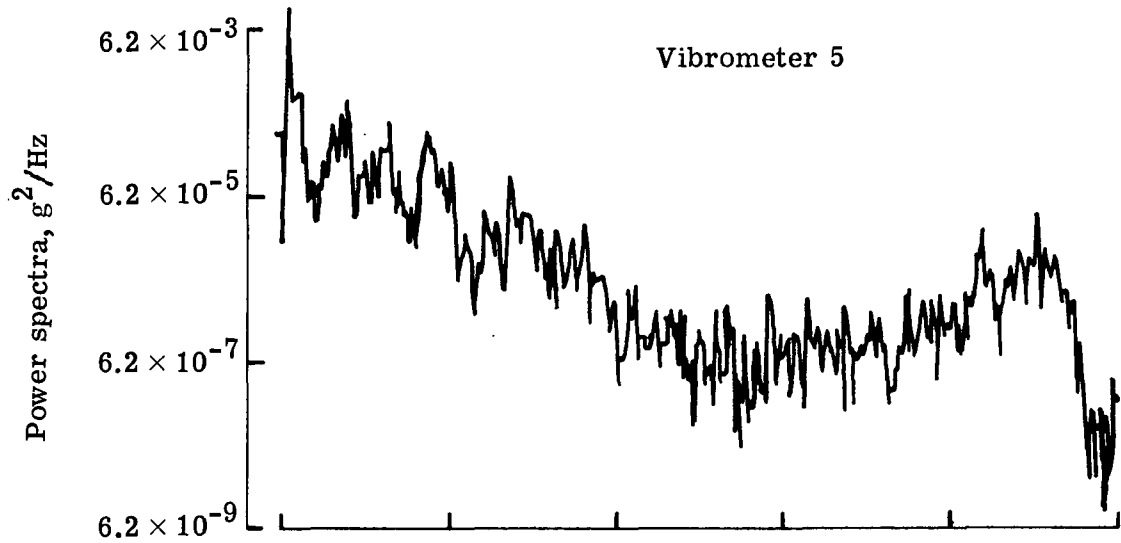


Figure 11.- Continued.

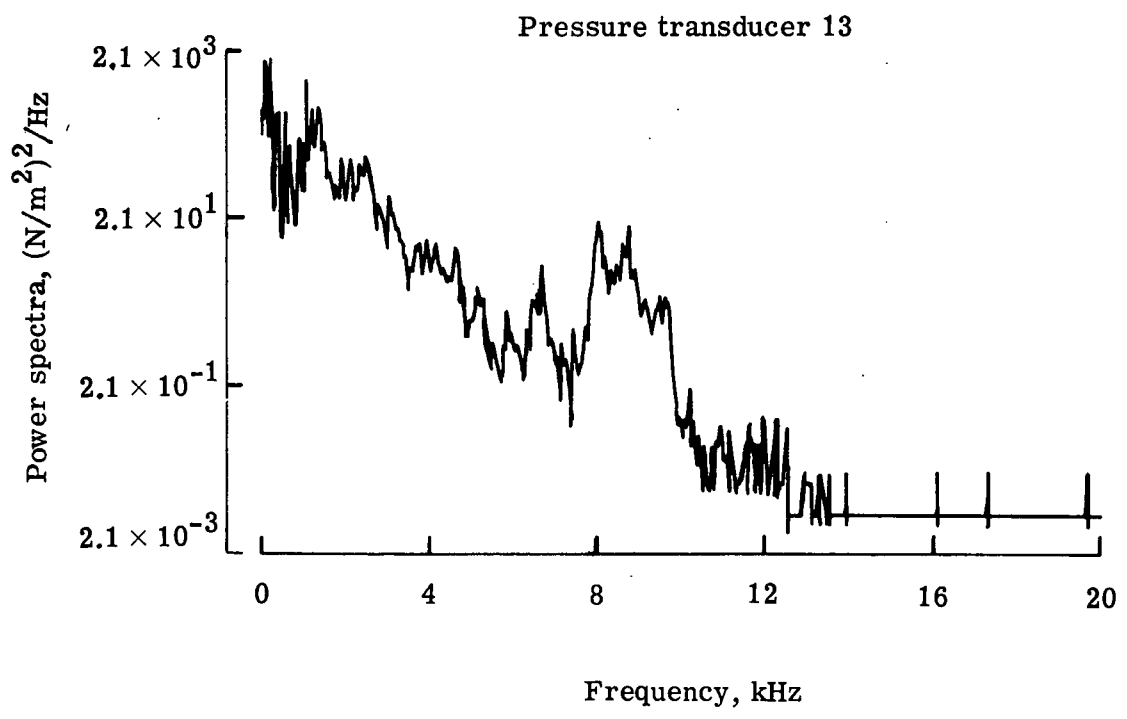
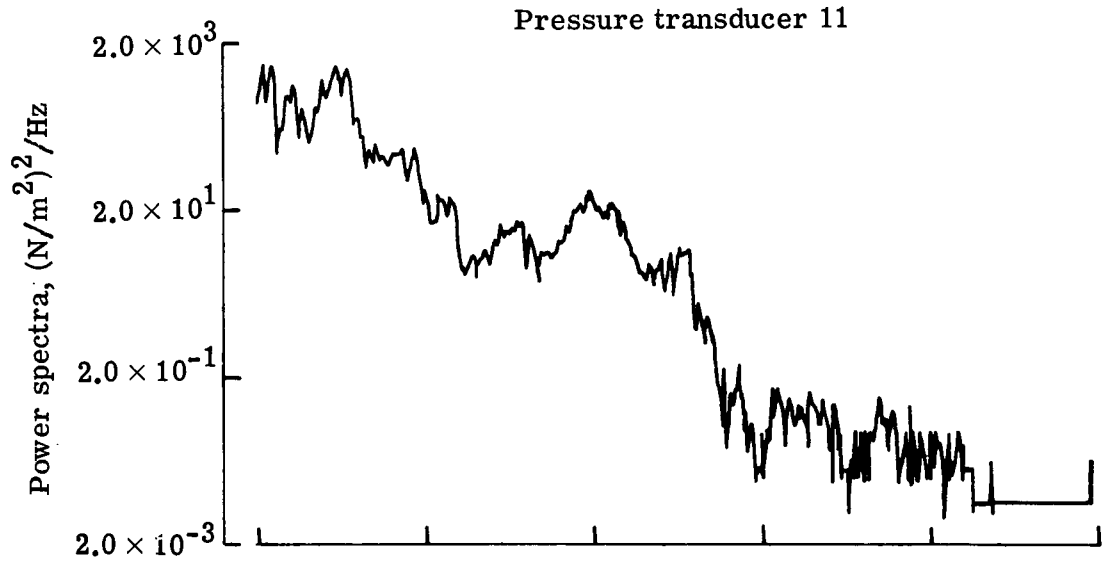


Figure 11.- Concluded.

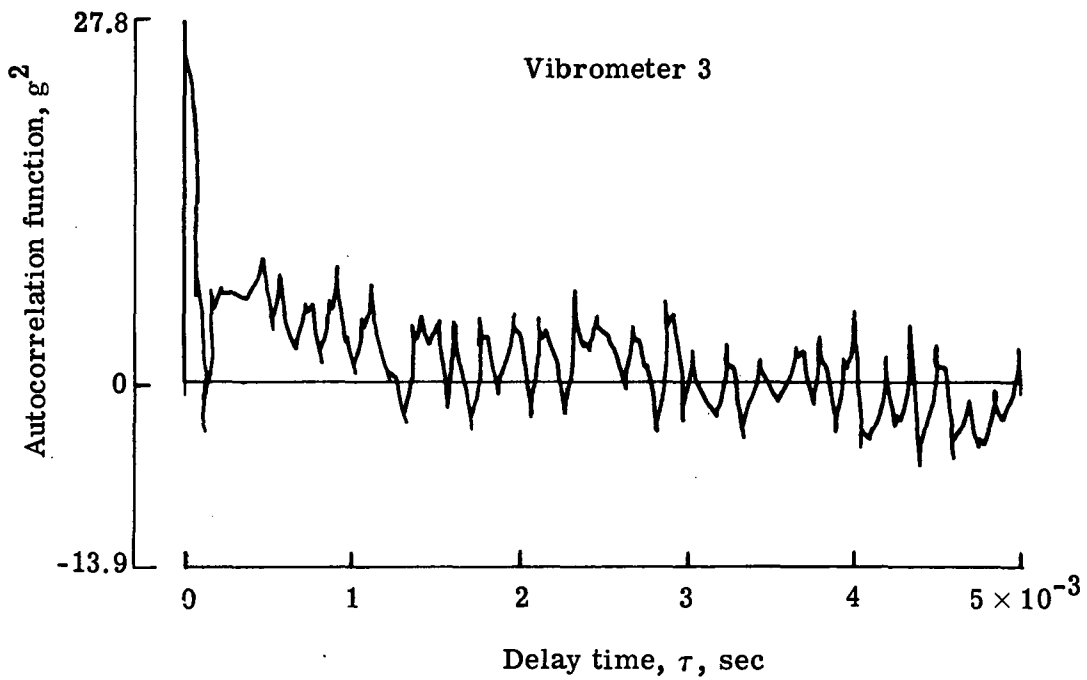
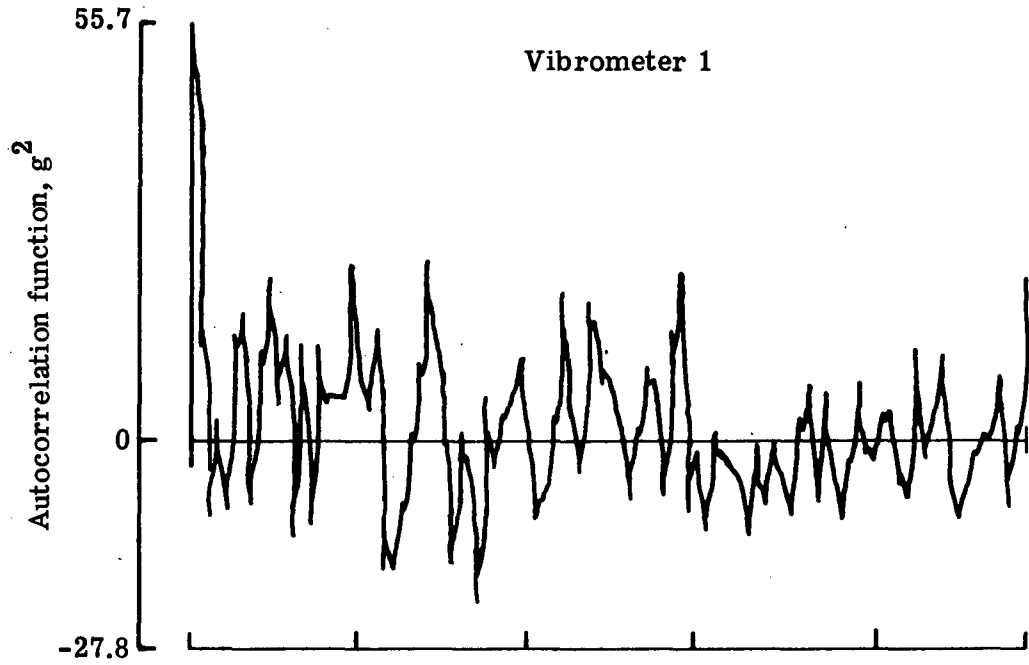


Figure 12.- Autocorrelation function for burn time 1.4 to 2.2 sec.

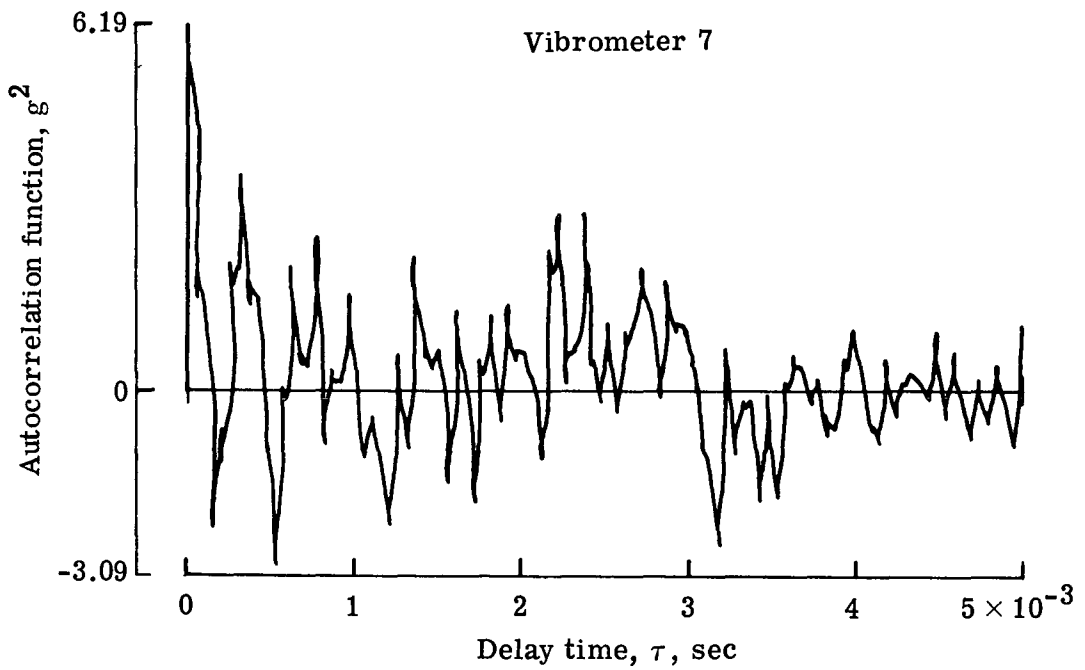
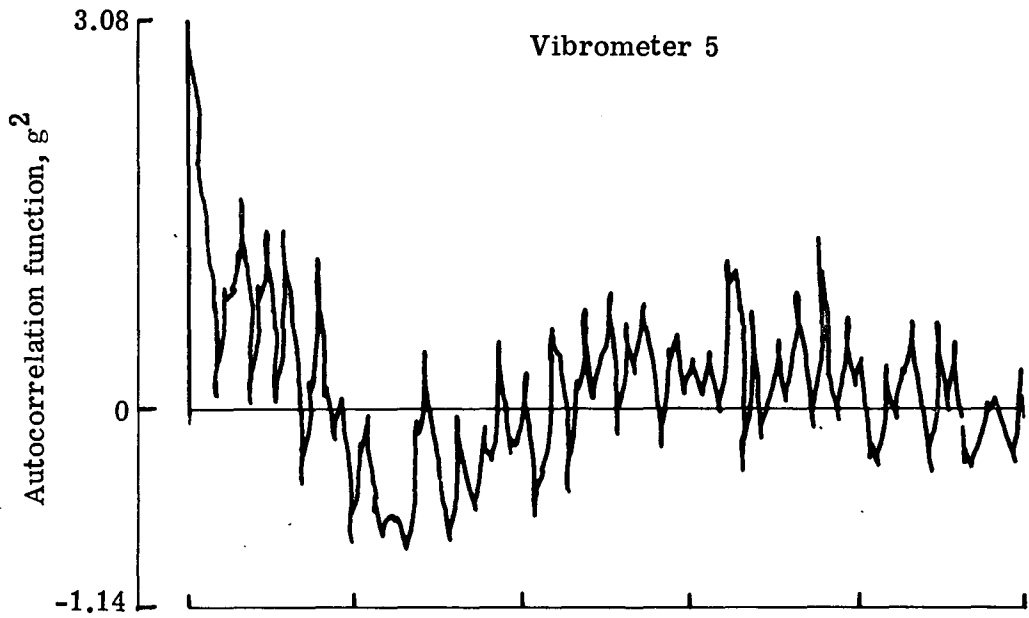


Figure 12.- Continued.

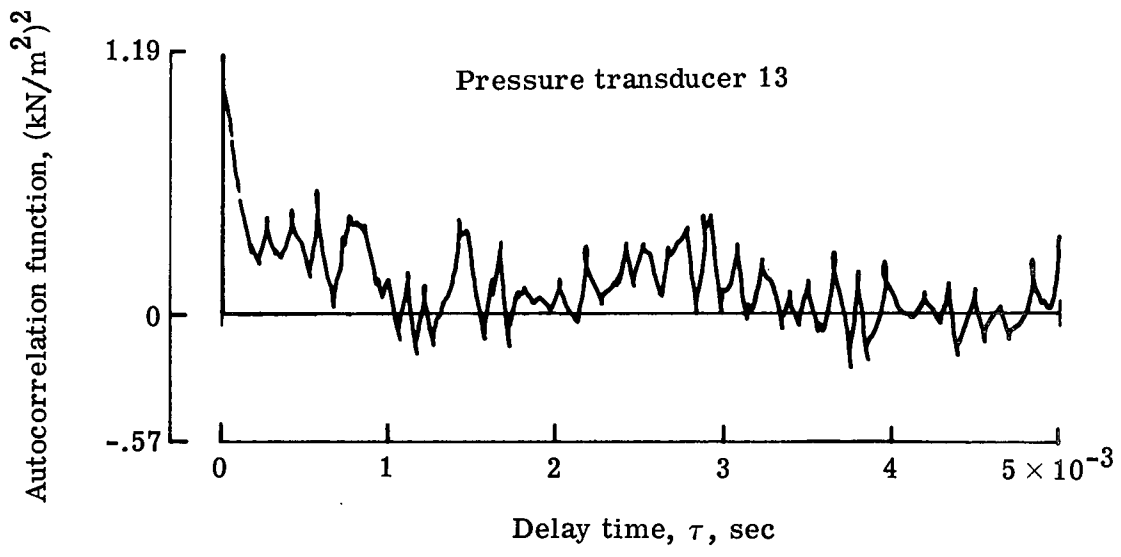
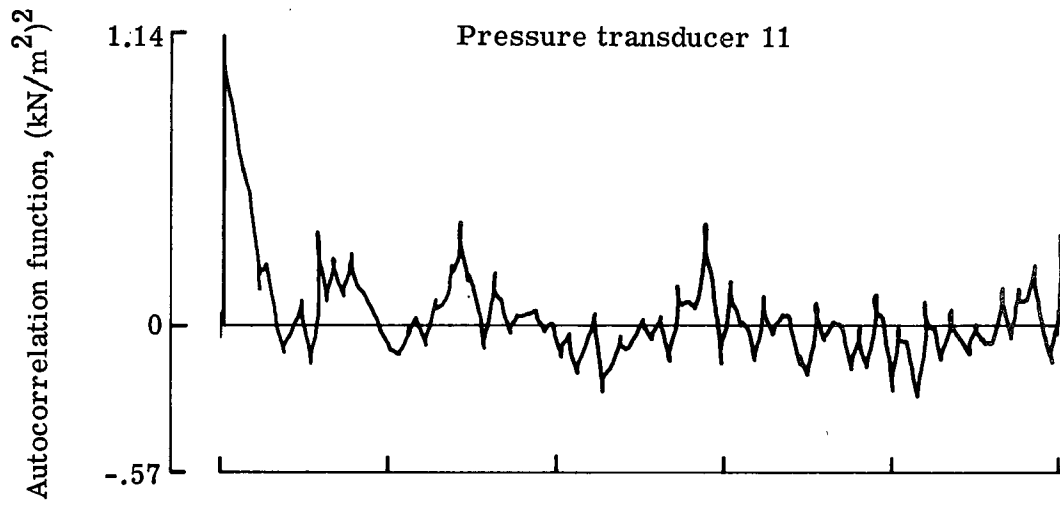


Figure 12.- Concluded.

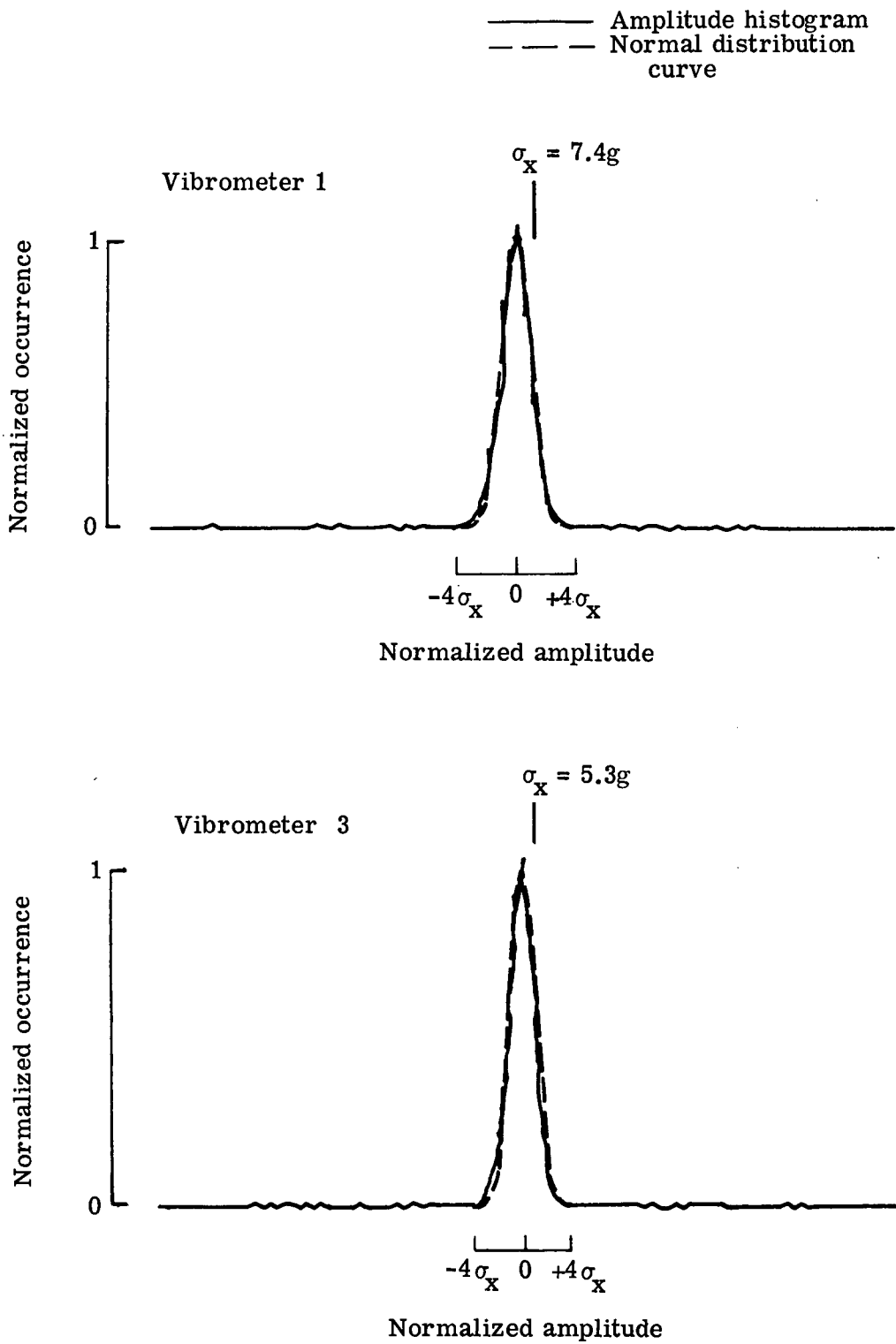


Figure 13.- Amplitude histogram for burn time 1.4 to 2.2 sec.

—— Amplitude histogram
- - - Normal distribution curve

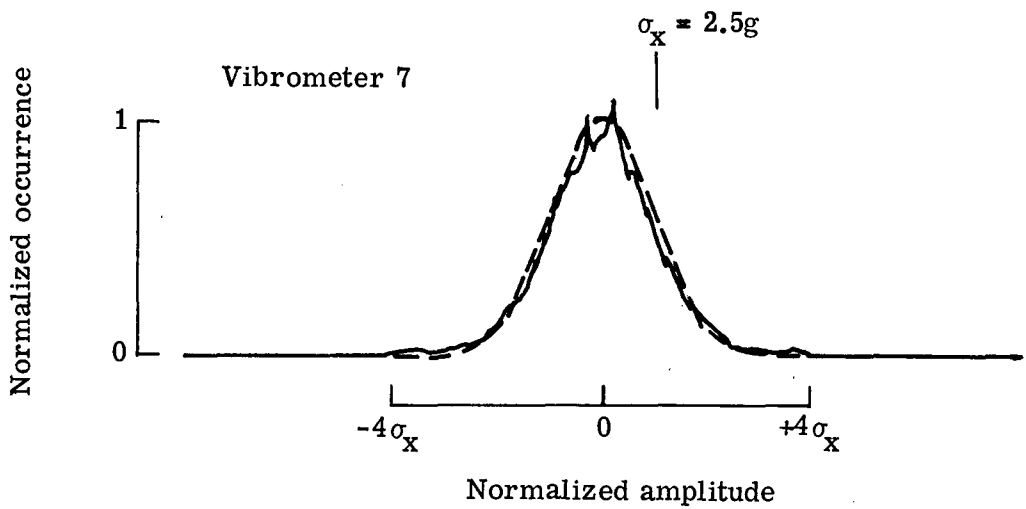
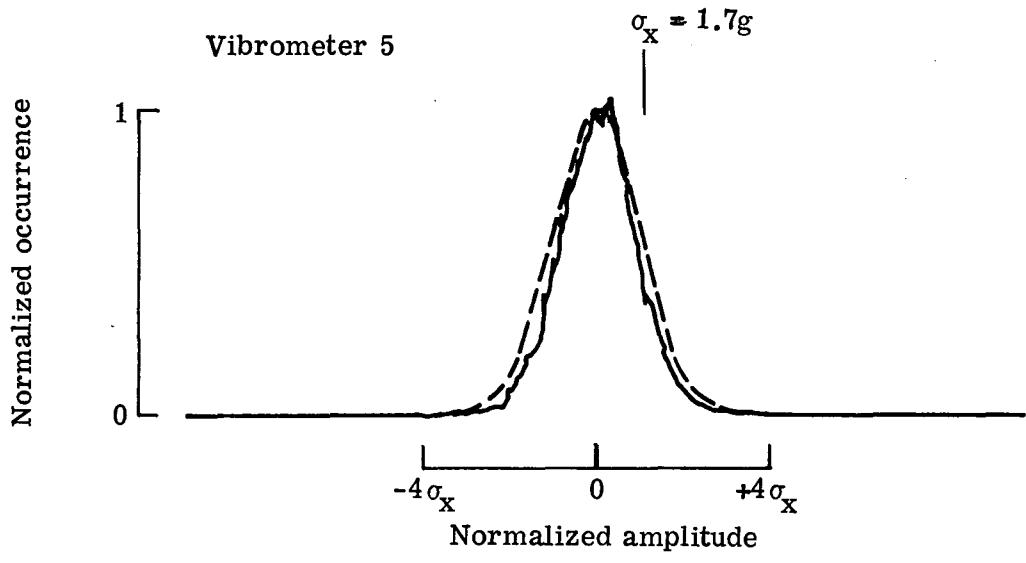


Figure 13.- Continued.

— Amplitude histogram
- - - Normal distribution curve

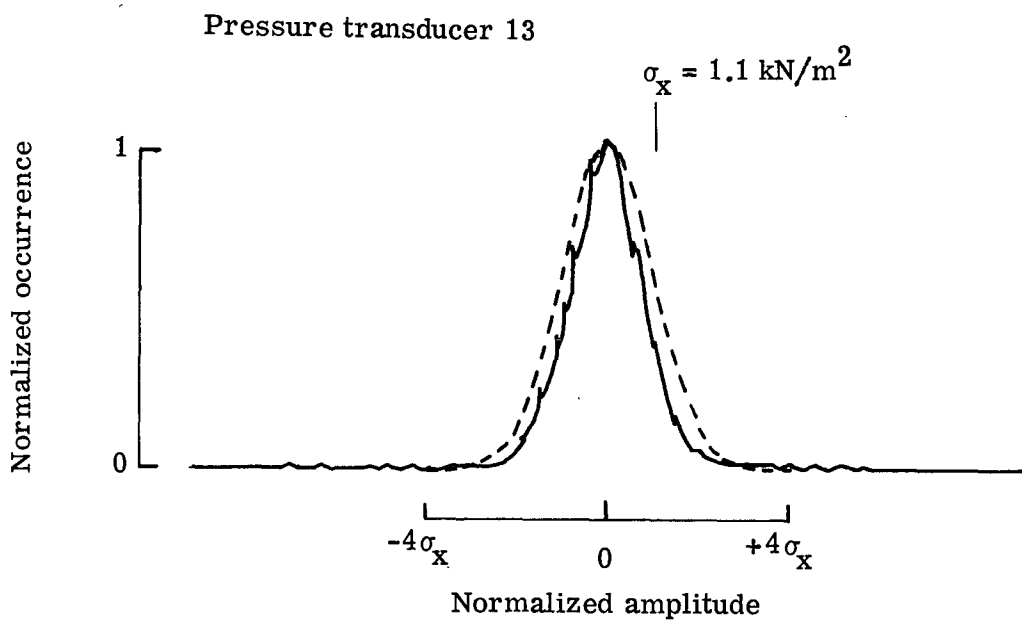
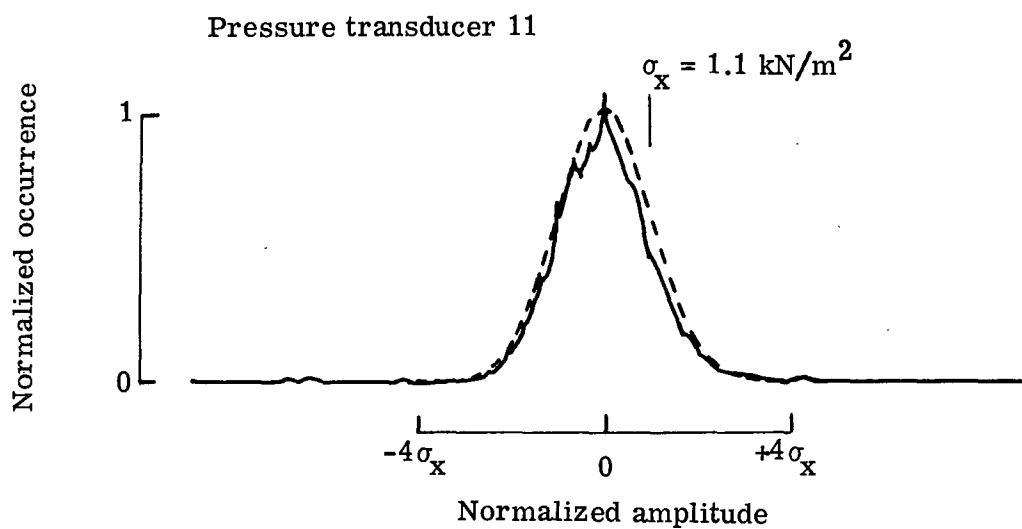


Figure 13.- Concluded.

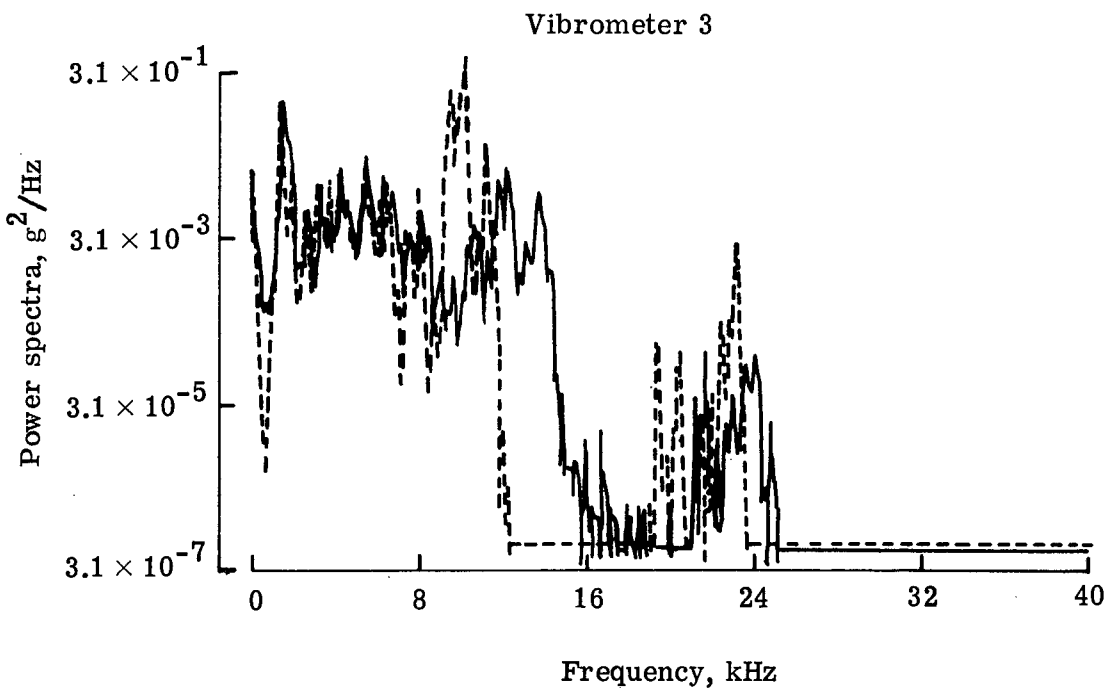
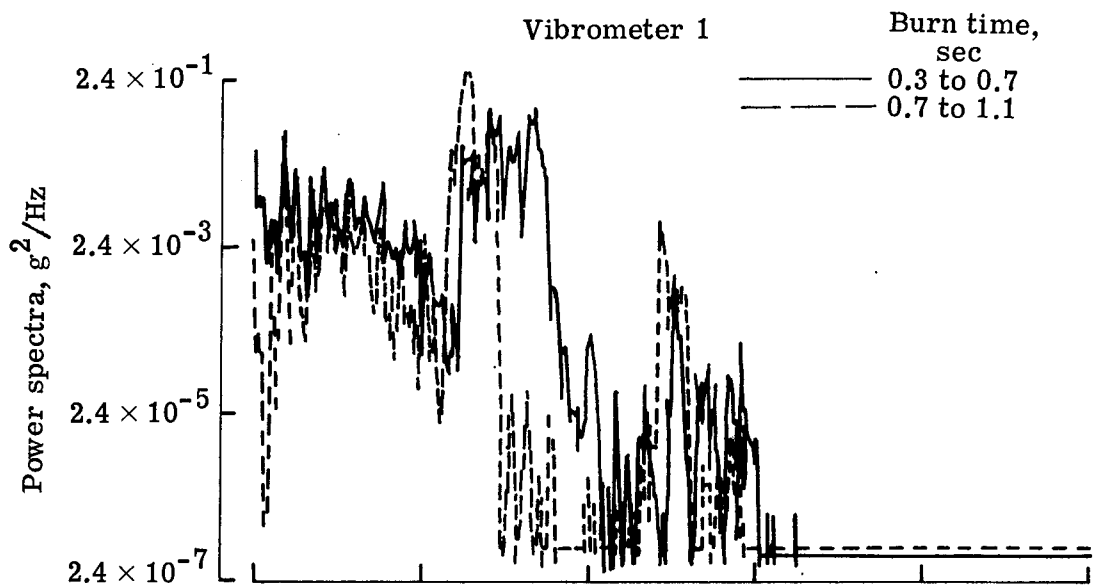


Figure 14.- Power-spectral-density measurements for burn times 0.3 to 0.7 sec and 0.7 to 1.1 sec.

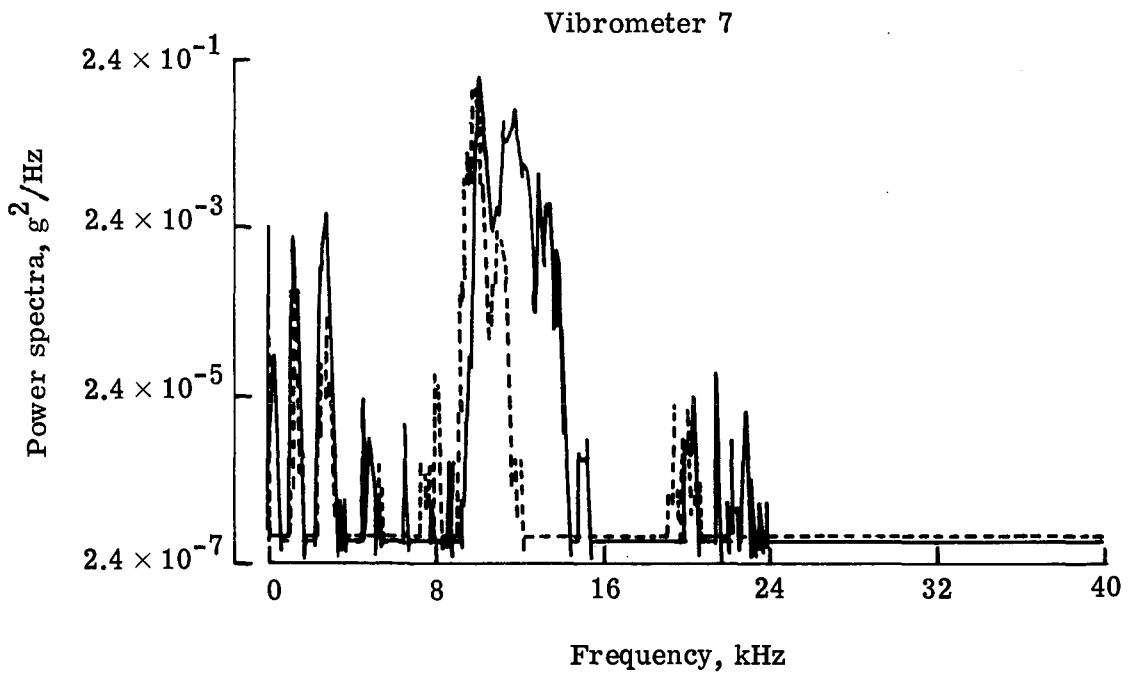
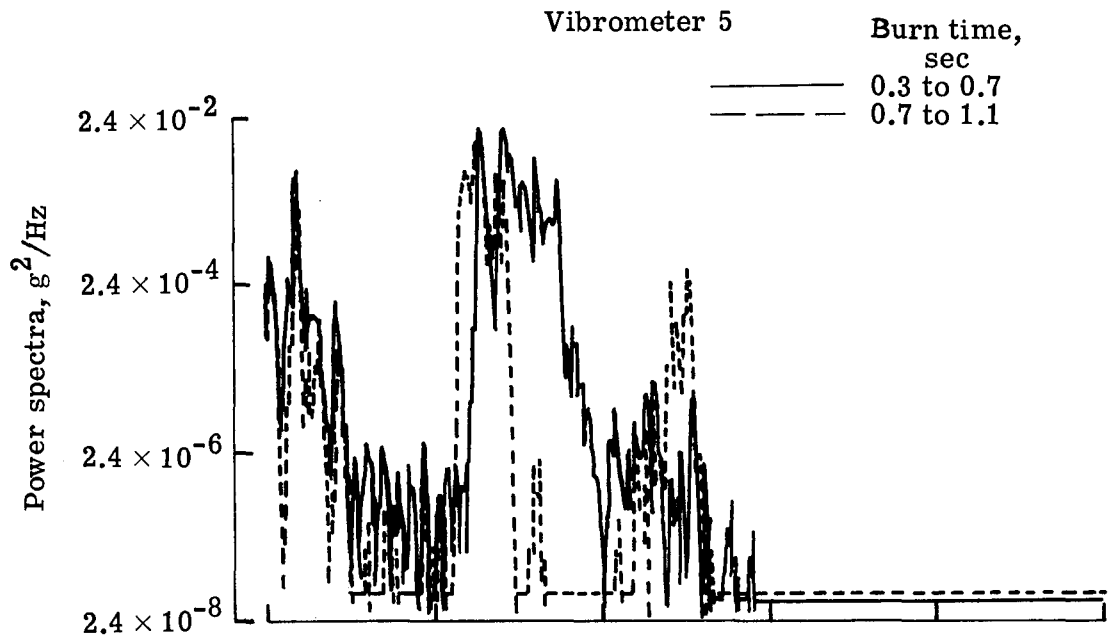


Figure 14.- Continued.

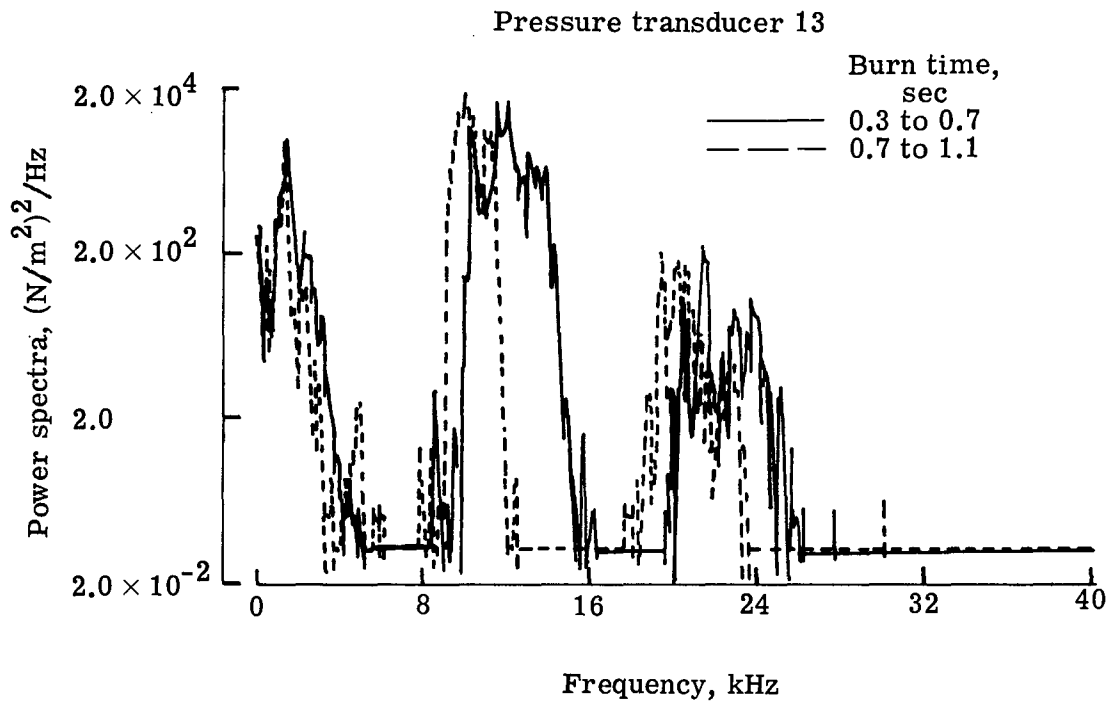


Figure 14.- Concluded.